A Ph.D. Dissertation entitled

Development of Portable Electrochemical Sensors: Miniaturization of Power Sources and Signal Detectors, and Improvement of Signal Sensitivities

휴대용 전기화학 센서의 개발: 전력원과 신호검출장치의 소형화, 집적화 및 신호 민감도 증진

August 2022

Graduate School of
Seoul National University
Electroanalytical chemistry

Song Yi Yeon

Development of Portable Electrochemical Sensors: Miniaturization of Power Sources and Signal Detectors, and Improvement of Signal Sensitivities

Name of Examiner: Taek Dong Chung

Submitting a Ph.D. Dissertation of Public Administration

August 2022

Graduate School of
Seoul National University
Major: Electroanalytical chemistry

Song Yi Yeon

Confirming the Ph.D. Dissertation written by
Song Yi Yeon
August 2022

Chair	황 윤 정	(Seal)
Vice Chair	정 택 동	(Seal)
Examiner	이 연	(Seal)
Examiner	김 종 원	(Seal)
Examiner	권 승 용	(Seal)

Abstract

Keyword : Portable sensors, reverse electrodialysis, electrochromic readout, bipolar electrodes, nanoporous electrodes
Student Number : 2016-24582

As the importance of point of care increases, many studies have been conducted on portable and wearable sensors. This dissertation introduces several strategies for the development of portable sensors. First, RED technology was used to miniaturize the power source that supplies voltage to the sensor. Miniaturized RED was designed for the voltage stability and convenience. Then, it was applied to a BPE sensor to implement a portable sensor. Second, an electrochromic glucose sensor was developed by designing a polyaniline based colorimetric readout system. Consequently, unlike conventional amperometric sensors, the glucose concentration could be measured in color signals without an extra current measurement. Lastly, nanoporous ITO was introduced to the BPE to enhance electrochemiluminescence signals, which are commonly used. As a result, sensitivity was improved according to the thickness of the porous layer. Through these studies, the development of portable sensors could be achieved as power sources and readout elements which are essential elements of electrochemical sensors were miniaturized and the signal intensities were highly improved.

Table of contents

List of Figures

List of Tables

Chapter 1. Introduction

1.1. General Introduction

Electrochemical sensors are applied extensively in diverse industries due to their advantages in sensitivity, portability, rapidness, low-cost and suitability for in-situ measurements.[1] Various types of analytes, such as metabolites, nucleic acids, proteins, and ions have been analyzed. First, the amperometric sensor, a representative electrochemical sensor, measures the analytes concentration by using the fact that the magnitude of the current is proportional to the concentration when the reactant is oxidized or reduced at the electrode under a constant potential.[2] If the reactant is redox active, it is oxidized or reduced on the electrode, and if not, the product generated through the enzyme reaction may also react at the electrode. For example, hydrogen peroxide is a commonly used reactant which is produced from enzymatic reactions of metabolites such as glucose and lactate,[3–5] and is commonly used in biosensors and immunosensors. Second, another representative electrochemical sensor, the potentiometric sensor is mainly used to analyze ion concentrations with voltage signals generated from selective membranes.[6] Voltage changes according to differences in ion concentrations across the ion selective membrane with Nernstian slope (59 mV/decade). Recently, solid contact ISEs[7–10] and miniaturized ISEs[11–13] have gained widespread interest. Besides, there are other methods of analysis in the electrochemical sensoring, such as electrochemical impedimetric sensors[14–16] and conductometric sensors.[17,18]

Since point of care (POC) was first introduced in early 1980's, lots of studies have been conducted.[19–23] The main concept is that people can rapidly check their health conditions regardless of time and place. In order to implement this concept, it is essential to develop a highly portable sensor. In addition, it should be easy to use and

the results should be obtained quickly. Therefore, recently in electrochemical sensor fields, a lot of studies have been reported to develop portable sensors with short detection times.[24–27] The studies on the materials, self-powered systems, and detecting strategies for the portable sensors are introduced below.

First, electrochemical sensors using portable materials such as paper, polymer, and textile have been developed. Being light and eco-friendly, paper has been extensively utilized as the material of choice for cost-effective sensor platforms. In particular, since the demonstration by Whitesides,[28–31] numerous studies on the development of paper-based electrodes as an alternative to traditional electrochemical sensors have been reported in regard to field diagnosis concerning environmental and health issues.[32–36] Microfluidic analytical devices (μPAD)[37] were reported as novel tools capable of analyzing small amounts of samples with low cost. Polymers also drew attentions due to the possibility of integrating them with wearable devices. Wax printing on polyethylene terephthalate was also used to make microchannels.[38] Polyimide,[39] polycarbonate,[40] poly (methyl methacrylate) (PMMA),[41] and polydimethylsiloxane (PDMS)[42] were used as the substrate of the devices. Although paper and polymers are the two most commonly used substrates, textiles such as fibers and fabrics have also been used to create portable devices, whereclothes,[43,44] tattoo,[45–47] lens,[48,49] and patch[50,51] type wearable sensors had been reported. However, in these systems, although the substrates were changed to a lighter material, most of them were still connected to external power sources or detectors.

Second, self-powered systems were first proposed by Zhong Lin Wang in 2006.[52] Piezoelectric nanogenerator (PENG) was developed,[52] which is a technology to convert motion energy to electricity. Zinc oxide nanowires were used to respond to external stimulation and generate voltage. Vibration energy and hydraulic energy

were also converted to electricity through PENG. Flexible e-skin was implemented for tactile perception and self-cleaning.[53] Furthermore, triboelectric nanogenerator (TENG) which generates electricity from mechanical compression between two different materials was developed.[54] TENG device was integrated with machine learning to recognize gestures and demonstrate VR control.[55] Meanwhile, energy harvesting from biological fluids with biofuel cell system was reported recently.[56] Wearable sweat sensors powered by BFC was introduced as a battery-free microfluidic/electronic system.[57]

Recently, studies have also been conducted on wireless transmission to increase portability by separating the detector that analyzes the sensor's signal from the sensor. The system can be particularly useful for patients suffering from diseases which require constant monitoring of physiological parameters. Mobile communication technologies such as fifth-generation wireless transmission and the Internet of things (IoT) were integrated with POC devices. Near-field communication was used to develop miniaturized and low-cost devices for sensing of the concentration of electrolyte levels in sweat.[57] Furthermore, wireless transmission technologies was applied to TENG to extend application of self powered systems.[58,59] The pulsed voltage generated from TENG was wirelessly transmitted to a receiver coil by a magnetic resonance-based wireless TENG.[60]

In summary, numerous studies have been conducted in various aspects for the development a portable sensor suitable for POC. However, these studies still need to go further to reach the actual utilization stage. Studies that have developed substrates using portable materials lack portability because they still use conventional power sources or detectors. Self-powered system like TENG and BFC can produce power from working environments such as biofluid and motion. However, in the case of

biofluid, extra energy storage devices are used because stable power generation is difficult,[56] and in the case of TENG, most of them have been limitedly used only for motion sensing. Wireless transmission is based on inductive coupling, so distance range is limited and depends on the size and shape of used antenna.[60] Therefore, unlike the strategies used in previous studies for POC, this dissertation focused on miniaturizing power sources and readout system. Furthermore, enhancing sensitivity will contribute to the ability to distinguish signals such as ECL with the naked eye without a separate image processing.

Nowadays, electrochemical sensors are no longer developed at the laboratory scale, but are required to move to commercial markets. Medical, environmental, pharmaceutical and food industry demand simple and fast sensors for diverse analytes for POC. As introduced above, studies that have been conducted in various aspects have developed so far. In the future, it is predicted that sensors suitable for POC will be developed when these kinds of research are converged like that the combination of a self-powered system with wireless transmission. Therefore, in this dissertation, I introduce my studies on the development of portable sensors for POC by miniaturizing and combining power source and detecting readout.

1.2. Background

1.2.1. Reverse electrodialysis

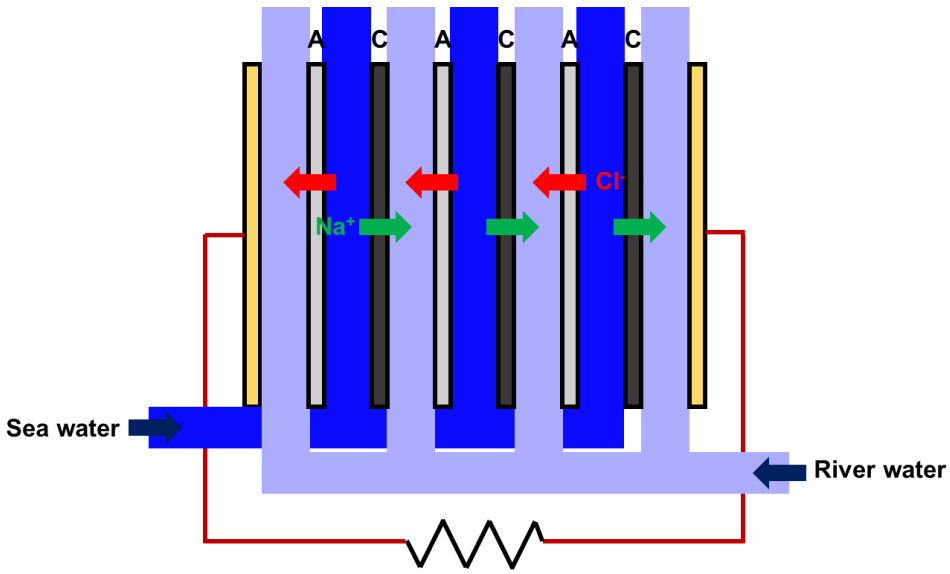

Figure 1-1. Schematic diagram of a reverse electrodialysis.

Reverse electrodialysis (RED) is the sustainable energy generating technology from salinity gradient between sea water and river water. Concentration difference of two solutions is converted to electrical energy. A RED stack consists of alternating anion exchange membranes and cation exchange membrane. (**Figure 1-1**) Sea water and river water alternately flow through the chamber between the membranes. Membrane potential is generated at each membrane and when membranes are stacked, this potential is summed. Thus, total voltage is determined by the concentration ratio of two solutions and the number of membranes.

$$E = N\frac{\alpha RT}{nF} ln \frac{a_H}{a_L} \qquad (1)$$

N is number of membrane, α is membrane permselectivity, F is Faraday constant, n is electrochemical valence, a_H is activity of the concentrated solution and a_L is

activity of the diluted solution.

1.2.2. Bipolar electrode

When an electronic conductor, BPE, is oriented in the opposite polarity applied with the driving electrodes, faradaic reactions occur at the two ends of the BPE. There is no electrical connection between the BPE and driving electrodes. BPE is mostly located inside microchannel which has a high resistance.

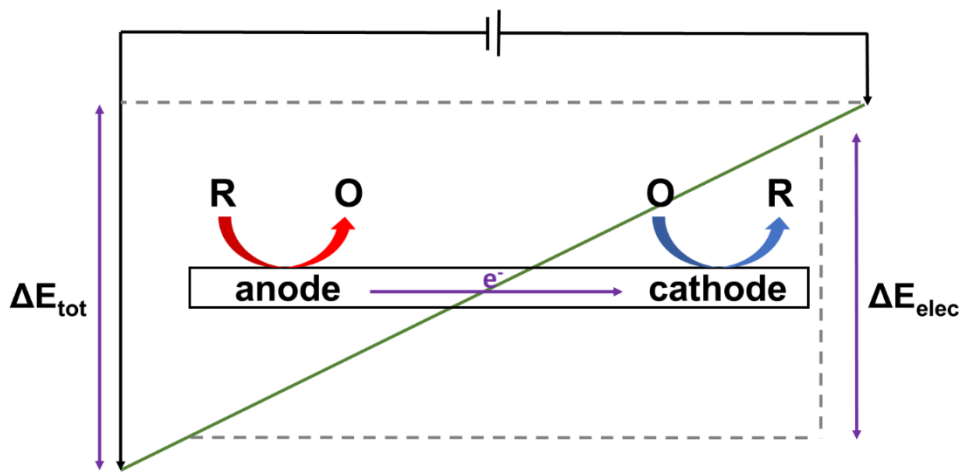

Figure 1-2. Schematic diagram of bipolar electrode.

As shown in **Figure 1-2**, total applied voltage E_{tot} is linearly diminished along the electrolyte channel. E_{tot} induces the BPE potential to float to an equilibrium potential (E_{elec}). The potential difference between the BPE and the solution at the two ends depend on length of the BPE, and it induces electrical reactions. Sum of cathodic overpotential and anodic overpotential ($\triangle E_{elec}$) is calculated as in equation (2).

$$\Delta E_{elec} = \frac{E_{tot}}{l_{channel}} l_{elec} \qquad (2)$$

Oxidative current and reductive current are equal according to electroneutrality. From this principle, BPE has been implemented in electroanalytical sensors. Sensing and reporting poles are coupled as the same current passes through the BPE. For example, analyte is reduced at the cathodic pole, then proportional reporting oxidation is occurred at the anodic pole. The most commonly used reporting reaction is electrochemiluminescence as explained below.

1.2.3. Electrochemiluminescence of $Ru(bpy)_3$

Electrochemiluminescence of excited ruthenium (II) complex has been well-documented. When a coreactant that provides oxidant or reductant intermediates present, ECL can be generated. Tris(2,2′-bipyridine)ruthenium(II) ($Ru(bpy)_3^{2+}$) with tripropylamine (TPA) as the coreactant is a commonly used redox system. As introduced below, $Ru(bpy)_3^{2+}$ is oxidized and then reduced by the TPA intermediate which is produced at the electrode.[61] In this process, excited state of $Ru(bpy)_3^{2+}$ is formed, resulting in the ECL emission. Consequently, $Ru(bpy)_3^{2+}$ is regenerated. The intensity of ECL is proportional to the generated current.

$$Ru(bpy)_3^{2+} \rightarrow Ru(bpy)_3^{3+} + e^-$$

$$Ru(bpy)_3^{3+} + Pr_3N \rightarrow Ru(bpy)_3^{2+} + Pr_3N^{\cdot+}$$

$$Pr_3N^{\cdot+} \rightarrow Pr_2N\dot{C}HEt + H^+$$

$$Ru(bpy)_3^{3+} + Pr_2N\dot{C}HEt \rightarrow Ru(bpy)_3^{2+*} + Pr_2N^+{=}CHEt$$

$$Ru(bpy)_3^{2+*} \rightarrow Ru(bpy)_3^{2+} + h\nu$$

(where $Pr = CH_3CH_2CH_2$- and $Et = CH_3CH_2$-)

1.2.4. Nanoconfinement effect of nanoporous ITO

Nanoporous electrodes were widely applied in energy conversion, electrochemical sensors and storage fields. They have received much attention because of their catalytic effect from their geometry. According to previous reports, electrocatalytic effects were commonly explained based on increased surface area, crystalline facet or surface defects. In addition to these adsorption-based mechanisms, there may be non-adsorption mechanisms that play an important role in catalytic properties of nanoporous electrodes. One of the key factors explaining the non-adsorption mechanism is the geometric effect of the confined space formed on the nanoporous electrode. To prove this, nanoporous ITO made by changing the thickness of the porous layer were fabricated and analyzed with electrochemical impedance spectroscopy (EIS).[62] It has been reported that the standard rate constant of $Fe^{2+/3+}$ is obtained through EIS fitting, and the thicker the porous layer, the larger the rate constant. This is because a thicker porous layer results in a longer pore pathway. Reactants which are in a deeper porous layer are more difficult to escape into the bulk and thus lead to a higher collision frequency with the electrode surface. This effect is called the ‘nanoconfinement effect’.

1.3. Purpose of Research

Electrochemical sensors measure various kinds of material concentrations through signals such as current, voltage, and impedance signals. Recently, as the interest of point of care has been increased, many studies have been conducted to increase the portability of electrochemical sensors. However, as mentioned in 1.1, the strategies used in previous studies still have limitations to be solved.

The electrochemical sensor basically consists of a power source, sensing component, and detector. Thus, the portability of these elements determines the overall portability. Unlike previous studies, research introduced in this dissertation focuses strategies to miniaturize power sources or detectors and integrate them into the sensors. In addition, sensitivity is a very important factor in terms of lowering the LOD, but signal enhancement is also required to observe signals with the naked eye without using an extra detector for the development of portable sensors.

Therefore, this dissertation deals with miniaturizing both amperometric sensors and potentiometric sensors, and enhancing the ECL signal of bipolar electrode sensors. First, Chapter 2 deals with the development of miniaturized RED for miniaturization of power sources. In addition, strategies that increases its voltage stability and convenience are introduced. Chapter 3 deals with the paper based electrochromic glucose sensor. A colorimetric readout based on polyaniline is developed to measure the current signal without using an extra instrument. Chapter 4 introduces a study that enhanced ECL signal by using nanoporous ITO in BPE sensors. Consequently, LOD and sensitivity are improved compared to the existing flat ITO-based BPE sensor.

1.4. References

(1) O. Kanoun, T. Lazarević-Pašti, I. Pašti, S. Nasraoui, M. Talbi, A. Brahem, A. Adiraju, E. Sheremet, R. D. Rodriguez, M. Ben Ali and A. Al-Hamry, *Sensors*, , DOI:10.3390/s21124131.

(2) D. Compagnone, *Electroanalysis*, 2012, **24**, 717.

(3) L. Cui, H. Yin, J. Dong, H. Fan, T. Liu, P. Ju and S. Ai, *Biosens. Bioelectron.*,

2011, **26**, 3278–3283.

(4) B. Xu, M. L. Ye, Y. X. Yu and W. De Zhang, *Anal. Chim. Acta*, 2010, **674**, 20–26.

(5) J. Liu, M. Zhang, J. Liu and J. Zheng, *Anal. Methods*, 2016, **8**, 1084–1090.

(6) E. Zdrachek and E. Bakker, *Anal. Chem.*, 2019, **91**, 2–26.

(7) U. Vanamo and J. Bobacka, *Electrochim. Acta*, 2014, **122**, 316–321.

(8) J. Kozma, S. Papp and R. E. Gyurcsányi, *Electrochem. commun.*, 2021, **123**, 106903.

(9) M. Rutkowska, T. Lindfors, Z. Boeva and M. Strawski, *Sensors Actuators, B Chem.*, 2021, **337**, 129808.

(10) A. W. Weber, G. D. O'Neil and S. P. Kounaves, *Anal. Chem.*, 2017, **89**, 4803–4807.

(11) M. P. S. Mousavi, M. K. Abd El-Rahman, E. K. W. Tan, H. H. Sigurslid, N. Arkan, J. S. Lane, G. M. Whitesides and P. Bühlmann, *Sensors Actuators, B Chem.*, 2019, **301**, 127112.

(12) Z. Zhang and I. Papautsky, *Electroanalysis*, 2021, **33**, 2143–2151.

(13) M. Novell, T. Guinovart, I. M. Steinberg, M. Steinberg, F. X. Rius and F. J. Andrade, *Analyst*, 2013, **138**, 5250–5257.

(14) A. Erdem and E. Eksin, *Biosensors*, 2020, **10**, 1–11.

(15) M. Xu and V. K. Yadavalli, *ACS Sensors*, 2019, **4**, 1040–1047.

(16) S. Brosel-Oliu, O. Mergel, N. Uria, N. Abramova, P. Van Rijn and A. Bratov, *Lab Chip*, 2019, **19**, 1436–1447.

(17) N. Kolahchi, M. Braiek, G. Ebrahimipour, S. O. Ranaei-Siadat, F. Lagarde and N. Jaffrezic-Renault, *J. Environ. Chem. Eng.*, 2018, **6**, 478–484.

(18) O. V. Soldatkina, O. O. Soldatkin, T. P. Velychko, V. O. Prilipko, M. A.

Kuibida and S. V. Dzyadevych, *Bioelectrochemistry*, 2018, **124**, 40–46.

(19) S. U. Son, S. B. Seo, S. Jang, J. Choi, J. woo Lim, D. K. Lee, H. Kim, S. Seo, T. Kang, J. Jung and E. K. Lim, *Sensors Actuators, B Chem.*, 2019, **291**, 257–265.

(20) W. Zhang, R. Wang, F. Luo, P. Wang and Z. Lin, *Chinese Chem. Lett.*, 2020, **31**, 589–600.

(21) B. Reddy, U. Hassan, C. Seymour, D. C. Angus, T. S. Isbell, K. White, W. Weir, L. Yeh, A. Vincent and R. Bashir, *Nat. Biomed. Eng.*, 2018, **2**, 640–648.

(22) Z. S. Ballard, H. A. Joung, A. Goncharov, J. Liang, K. Nugroho, D. Di Carlo, O. B. Garner and A. Ozcan, *npj Digit. Med.*, 2020, **3**, 1–8.

(23) A. Kaushik and M. A. Mujawar, *Sensors (Switzerland)*, 2018, **18**, 10–13.

(24) A. K. Kaushik, J. S. Dhau, H. Gohel, Y. K. Mishra, B. Kateb, N. Y. Kim and D. Y. Goswami, *ACS Appl. Bio Mater.*, , DOI:10.1021/acsabm.0c01004.

(25) E. T. S. G. da Silva, D. E. P. Souto, J. T. C. Barragan, J. de F. Giarola, A. C. M. de Moraes and L. T. Kubota, *ChemElectroChem*, 2017, **4**, 778–794.

(26) B. Chakraborty, A. Das, N. Mandal, N. Samanta, N. Das and C. R. Chaudhuri, *Sci. Rep.*, 2021, **11**, 1–12.

(27) A. Ramanujam, S. Almodovar and G. G. Botte, *Processes*, 2021, **9**, 1236.

(28) A. W. Martinez, S. T. Phillips, M. J. Butte and G. M. Whitesides, *Angew. Chemie - Int. Ed.*, 2007, **46**, 1318–1320.

(29) Z. Nie, C. A. Nijhuis, J. Gong, X. Chen, A. Kumachev, A. W. Martinez, M. Narovlyansky and G. M. Whitesides, *Lab Chip*, 2010, **10**, 477–483.

(30) A. W. Martinez, S. T. Phillips and G. M. Whitesides, *Proc. Natl. Acad. Sci. U. S. A.*, 2008, **105**, 19606–19611.

(31) F. Güder, A. Ainla, J. Redston, B. Mosadegh, A. Glavan, T. J. Martin and G. M. Whitesides, *Angew. Chemie - Int. Ed.*, 2016, **55**, 5727–5732.

(32) Z. Yu, Y. Tang, G. Cai, R. Ren and D. Tang, *Anal. Chem.*, 2019, **91**, 1222–1226.

(33) W. J. Zhu, D. Q. Feng, M. Chen, Z. D. Chen, R. Zhu, H. L. Fang and W. Wang, *Sensors Actuators, B Chem.*, 2014, **190**, 414–418.

(34) R. Cánovas, M. Parrilla, P. Blondeau and F. J. Andrade, *Lab Chip*, 2017, **17**, 2500–2507.

(35) D. D. Liana, B. Raguse, J. J. Gooding and E. Chow, *ACS Appl. Mater. Interfaces*, 2015, **7**, 19201–19209.

(36) N. Colozza, K. Kehe, G. Dionisi, T. Popp, A. Tsoutsoulopoulos, D. Steinritz, D. Moscone and F. Arduini, *Biosens. Bioelectron.*, 2019, **129**, 15–23.

(37) K. Yamada, T. G. Henares, K. Suzuki and D. Citterio, *Angew. Chemie - Int. Ed.*, 2015, **54**, 5294–5310.

(38) A. Z. Qamar, G. Parker, G. R. Kinsel and M. H. Shamsi, *Microfluid. Nanofluidics*, 2019, **23**, 1–8.

(39) A. Weltin, J. Kieninger, B. Enderle, A. K. Gellner, B. Fritsch and G. A. Urban, *Biosens. Bioelectron.*, 2014, **61**, 192–199.

(40) E. L. Tur-García, F. Davis, S. D. Collyer, J. L. Holmes, H. Barr and S. P. J. Higson, *Sensors Actuators, B Chem.*, 2017, **242**, 502–510.

(41) N. Wongkaew, P. He, V. Kurth, W. Surareungchai and A. J. Baeumner, *Anal. Bioanal. Chem.*, 2013, **405**, 5965–5974.

(42) J. Wu, R. Wang, H. Yu, G. Li, K. Xu, N. C. Tien, R. C. Roberts and D. Li, *Lab Chip*, 2015, **15**, 690–695.

(43) A. Ancans, M. Greitans, R. Cacurs, B. Banga and A. Rozentals, *Sensors*,

2021, **21**, 1–16.

(44) I. Wicaksono, C. I. Tucker, T. Sun, C. A. Guerrero, C. Liu, W. M. Woo, E. J. Pence and C. Dagdeviren, *npj Flex. Electron.*, 2020, 4, 5.

(45) J. Kim, W. R. De Araujo, I. A. Samek, A. J. Bandodkar, W. Jia, B. Brunetti, T. R. L. C. Paixão and J. Wang, *Electrochem. commun.*, 2015, **51**, 41–45.

(46) A. J. Bandodkar, V. W. S. Hung, W. Jia, G. Valdés-Ramírez, J. R. Windmiller, A. G. Martinez, J. Ramírez, G. Chan, K. Kerman and J. Wang, *Analyst*, 2013, **138**, 123–128.

(47) A. J. Bandodkar, W. Jia, C. Yard, X. Wang, J. Ramirez and J. Wang, .

(48) J. Kim, M. Kim, M. S. Lee, K. Kim, S. Ji, Y. T. Kim, J. Park, K. Na, K. H. Bae, H. K. Kim, F. Bien, C. Y. Lee and J. U. Park, *Nat. Commun.*, **8**, 14997.

(49) M. Yuan, R. Das, R. Ghannam, Y. Wang, J. Reboud, R. Fromme, F. Moradi and H. Heidari, *Adv. Intell. Syst.*, 2020, **2**, 1900190.

(50) M. R. Ely, B. R. Ely, T. D. Chinevere, C. P. Lacher, H. C. Lukaski and S. N. Cheuvront, *Physiol. Meas.*, 2012, **33**, 385–394.

(51) A. Mena-Bravo and M. D. Luque de Castro, *J. Pharm. Biomed. Anal.*, 2014, **90**, 139–147.

(52) Z. L. Wang and J. Song, *Science (80-.).*, 2006, **312**, 242–246.

(53) H. He, Y. Fu, W. Zang, Q. Wang, L. Xing, Y. Zhang and X. Xue, *Nano Energy*, 2017, **31**, 37–48.

(54) F. R. Fan, Z. Q. Tian and Z. Lin Wang, *Nano Energy*, 2012, **1**, 328–334.

(55) F. Wen, Z. Sun, T. He, Q. Shi, M. Zhu, Z. Zhang, L. Li, T. Zhang and C. Lee, *Adv. Sci.*, 2020, **7**, 1–15.

(56) J. Lv, I. Jeerapan, F. Tehrani, L. Yin, C. A. Silva-Lopez, J. H. Jang, D. Joshuia, R. Shah, Y. Liang, L. Xie, F. Soto, C. Chen, E. Karshalev, C.

Kong, Z. Yang and J. Wang, *Energy Environ. Sci.*, 2018, **11**, 3431–3442.

(57) A. J. Bandodkar, P. Gutruf, J. Choi, K. H. Lee, Y. Sekine, J. T. Reeder, W. J. Jeang, A. J. Aranyosi, S. P. Lee, J. B. Model, R. Ghaffari, C. J. Su, J. P. Leshock, T. Ray, A. Verrillo, K. Thomas, V. Krishnamurthi, S. Han, J. Kim, S. Krishnan, T. Hang and J. A. Rogers, *Sci. Adv.*, 2019, **5**, 1–16.

(58) X. Cao, M. Zhang, J. Huang, T. Jiang, J. Zou, N. Wang and Z. L. Wang, *Adv. Mater.*, 2018, **30**, 1–8.

(59) Y. Jie, J. Ma, Y. Chen, X. Cao, N. Wang and Z. L. Wang, *Adv. Energy Mater.*, 2018, **8**, 1–7.

(60) C. Zhang, J. Chen, W. Xuan, S. Huang, B. You, W. Li, L. Sun, H. Jin, X. Wang, S. Dong, J. Luo, A. J. Flewitt and Z. L. Wang, *Nat. Commun.*, 2020, **11**, 58.

(61) S. Y. Yeon, J. Yun, S. Yoon, D. Lee, W. Jang, S. H. Han, C. M. Kang and T. D. Chung, *Chem. Sci.*, 2018, **9**, 8071–8076.

(62) M. Seo, J. H. Bae, D. W. Hwang, B. Kwak, J. Yun, S. Y. Lim and T. D. Chung, *Electrochim. Acta*, 2017, **258**, 90–97.

Chapter 2. Development of miniaturized reverse electrodialysis battery

Parts of this chapter were published as S. Y. Yeon[1]; J. Yun[1]; S. Yoon; D. Lee; W. Jang; S. H. Han; C. M. Kang; T. D. Chung*. "A miniaturized solid salt reverse electrodialysis battery: a durable and fully ionic power source" *Chem. Sci.* **2018**, *9(42)*, 8071-8076. S. Y. Yeon, J. Yun and T. D. Chung conceived the concept and designed the experiments. S. Y. Yeon. and J. Yun carried out the experiments. S. Y. Yeon designed the application system and J. Yun suggested the principle of PssRED operation.

2.1. Introduction

Vital to biological activity, ionic systems form the basis of physiological processes in all living organisms. Through tight regulation of ion transport, key biological processes are governed. For instance, nerve signals are transmitted via the potassium-sodium concentration gradients within nerve cells, and energy production is facilitated by a proton gradient which powers adenosine-triphosphate (ATP) synthesis.

Inspired by biological systems, completely ionic circuits have been developed to understand and control the behavior of ions, and to communicate between electronic circuits and organisms. Since Bockris first reported on electrolytic junctions,[1] various ionic device such as ionic diodes,[2,3] ionic transistors[4,5] and ionic logic gates[6-8] have been studied to precisely control the ionic species in the electrolyte. Based on the working principle of the aforementioned devices, a wide range of functional materials has been reported by researchers of inorganic and organic materials.[9,10] In line with these efforts, polyelectrolytes were proposed as an attempt to bridge the gap between solid electronic and ionic systems. These electronic components are flexible, light-weight, environmentally benign, and biocompatible,[2] with the aim of mounting on or implanting in the human body to perform various functions such as sensing, interfacing and drug delivery.

However, the ionic-electronic interfaces that apply electrical energy to an ionic environment present certain concerns. Firstly, the interfacial charge transfer, also known as the faradaic reaction, can potentially be unfavorable to the biosystem[11-14] and for analysis.[15] In addition, the conventional power sources are not bio-compatible because they require toxic materials and are not flexible. Thus, further

modification and careful design of power sources are required for them to be compatible with bio-electronic interfaces and disposable sensors. Therefore, a new concept of power source that generating ionic flow without causing bio-compatibility issues is in demand. To this end, for instance, electronic batteries which could serve as alternatives have been suggested using different electrode materials and ionic cables soaked with various ions which generates selective flux of Li^+, Na^+, K^+, Ca^{2+} ions.[16]

Towards this objective, I have focused on reverse electrodialysis (RED). Since the landmark proof-of-concept by Pattle in 1954,[17] RED has garnered widespread attention from researchers as a promising source of renewable energy which could harvest a large amount of electricity from the mixing of river and sea water.[18-21] In another aspect, RED is an ideal power source surrogate to couple with various ionic devices, since it can generate ionic electricity without the need of solid conductors such as metal electrodes.[22] However, the necessity of a mechanical pump to maintain the power of RED is cumbersome, as the ionic devices are usually incorporated within microchips. In our previous studies, we proved that miniaturized RED could drive a bipolar electrochemical sensor and an iontophoretic drug delivery device by solely ionic means.[23,24] However, rapid power decay in the absence of a pump and tedious injection of saline solutions to every chamber of the miniaturized RED have greatly hindered its practicality.

I, thus, wished to devise an ultimate miniaturized RED-based power source that could surmount the previous systems, named precipitation-assisted RED (PssRED, vide infra). If it could serve as an economical and convenient means to provide stable power over longer duration of time without the aid of a pump, I believed that it could potentially be coupled with various electronic devices to achieve practicality. The

operation of two completely ionic model device, bipolar electrode (BPE) based sensing apparatus and polyelectrolyte based ionic diode, is presented to highlight the utility of the newly developed PssRED system. BPEs, being electrically disconnected electrodes, are hence well-suited for miniaturized devices that are unwieldy for wiring. Therefore, bipolar electrode-electrochemiluminescence (BPE-ECL) sensing of many targets are intensively studied,[25-28] leading to a surge in demand for smaller, simpler, and lighter power sources.[29] Thus, here, I examine PssRED as a stable power source for the BPE sensing system by showcasing efficient quantification of important target analytes, benzyl viologen (BV),[25,30] a member of the viologen family in which various enzymatic redox mediators are included,[31,32] and H_2O_2,[33-35] a key indicator of cellular oxidation.[36] The second model system, the polyelectrolyte ionic diode, allows ionic current to be rectified, thus can model biological information processing.[22,30] These ionic circuits could serve as a key component for the construction of a biomimetic device for "iontronic" functions.[37] Such iontronic devices are envisioned to enable the merger of classical and bio-electronics by communicating between electronic devices and the biological system. I, therefore, demonstrate that PssRED could serve as an efficient power source for controlling ionic flow by manipulating the ionic distributions in the polyelectrolyte ionic diode. These two examples could confirm the suitability of PssRED as a durable power source for various devices that require an ionic power supply.

2.2. Experimental

2.2.1. Materials

All chemicals were used as received without further purification. Tris(2,2'-

bipyridyl)dichlororuthenium(II) hexahydrate ($Ru(bpy)_3Cl_2 \cdot 6H_2O$), tripropylamine (TPA), benzyl viologen, barium chloride, silver sulfate, diallyldimethylammonium chloride (DADMAC), 2-acrylamido-2-methyl-1-propanesulfonic acid (AMPSA), sodium chloride, potassium chloride, 2-hydroxy-4′-(2-hydroxyethoxy)−2-methylpropiophenone, fluorescein sodium salt, 3-(trimethoxysilyl)propyl methacrylate, methanol, silver wire (dia. 0.5 mm), platinum wire (dia. 0.5 mm), and indium tin oxide coated glass (ITO, 8-12 Ω/sq) were purchased from Sigma Aldrich (St. Louis, Missouri, U.S.A.). Ag/AgCl reference electrode was purchased from BASi (West Lafayette, Indiana, U.S.A.). Hexamethyldisilazane (HMDS), ethanol, hydrogen peroxide (30% aq.), sulfuric acid and acetone were obtained from J. T. Baker (Phillipsburg, New Jersey, U.S.A.). Photoresist (PR; AZ 4620) and developer (AZ 400K) were purchased from Merck (Kenilworth, NJ, U.S.A.). TIN etchant (TE-100) was purchased from Transene Company (Danvers, MA, U.S.A.). Anion exchange membrane (Selemion AMV) and cation exchange membrane (CMV) were products of Asahi Glass Co., Ltd. (Tokyo, Japan). Waterproof double-sided tape (ACE CROSS SBX) was purchased from Koyo-kagaku Co., Ltd. (Soka, Japan) and further customized by Teratec. (Daegu, Korea). Deionized water (18 MΩ·cm) was obtained from NANO pure Diamond (Barnstead, New Hampshire, U.S.A). Potentiostat (Reference 600, Gamry/CHI604 and CHI 750, CH Instrument), digital camera (Canon EOS 750D, ISO 6400), microscope (Nikon TE2000U) and PMT detector (H10722-20, Hamamatsu) were used for electrochemical and optical measurements.

2.2.2. Preparation of miniaturized solid salt RED

Miniaturized solid salt REDs were prepared by stacking cation exchange membranes (CEM) and anion exchange membranes (AEM) alternatively in two parallel columns, as shown in **Figure 2-1a**. Double-sided waterproof tape (4.0 × 2.0 cm^2, 250 μm/layer) were used as the template. A CEM and an AEM were attached over each hole of the waterproof tape, respectively. The high concentration and the low concentration chambers alternated between each layer. On the uppermost layer was placed three-layered waterproof tape with a rectangular chamber (3.0 × 1.0 cm^2) to connect the two columns. Salt powder was delivered using laboratory spatula without precise measurement, but sufficiently to reach saturation, when the membranes were stacked layer-by layer.

2.2.3. Characterization of the miniaturized solid salt REDs

For operation, the ssREDs were immersed into deionized or tap water, pressed and released with fingers to fill each layer. The performance of miniaturized ssRED was characterized by the four-electrode system. Current flowing through the RED cell was galvanostatically driven by two platinum wires connected to a potentiostat (Reference 600, Gamry), while the potential was measured by two Ag/AgCl reference electrodes with a second potentiostat (CHI604, CH Instrument). Current was gradually increased from 0 to 200 μA with a step size of 10 μA.

2.2.4. Fabrication of ITO electrode and BPE microchip

The BPE microchip consisted of the upper patterned glass and lower ITO-electrode-embedded glass. A slide glass was washed with piranha solution for 40 min and ITO-

coated glass was washed with ethanol, acetone, and deionized water, successively and baked at 150 °C for 15 min. HMDS was spin-coated on the glass surfaces and baked at 110 °C for 1.5 min. Then, PR (AZ 4620) was spin-coated and baked at 100 °C for 1.5 min. UV light (365 nm) was illuminated on the PR layer through a mask with a channel pattern and BPE masked pattern. Then the PR pattern was developed using AZ 400K developer and baked at 120 °C for 15 min. Upper glass was immersed in buffered oxide etchant for 45 min and lower ITO-coated glass was etched with TE-100. Four holes were drilled on upper glass for solution reservoirs. Finally, the glasses were sonicated in acetone and were both submerged in NH_4OH (30% aq.) : H_2O_2 (30% aq.) : D.I. water (2:1:2) solution at 180 °C for 30 min. They were heated to 500 °C in a furnace (CRF-M15, Ceber, Korea) for 12 h for complete attachment.

2.2.5. Electrochemical and optical analysis

Cyclic voltammetry was performed by a potentiostat (CHI750, CH Instruments). The three-electrode system consisted of ITO coated glass as the working electrode, Pt wire as the counter electrode, and Ag/AgCl as the reference electrode.

The reporting channel on the anodic side was filled with 0.1 M PBS (pH 6.9) containing 5 mM $Ru(bpy)_3Cl_2 \cdot 6H_2O$ and 25 mM TPA. The detecting channel for BV reduction on the cathodic side was filled with 0.1 M PBS (pH 6.9) containing different concentrations (0 to 10 mM) of BV. For detection of H_2O_2, it was filled with 0.1 M PBS (pH 6.9) containing different concentrations (0 to 10 mM) of H_2O_2. Constant voltage was applied to the both ends by either a potentiostat or a PssRED. When a potentiostat was used, potential was applied through Ag/AgCl driving

electrodes (diameter: 0.5 mm). Otherwise, activated PssRED was attached wirelessly to the BPE chip. For both cases, the ECL images were obtained in the dark room with an exposure time of 15 s using a digital camera (Canon EOS 750D, ISO 6400). ECL intensities of the images were analyzed by the ImageJ software.

2.2.6. Detection of ECL intensity by photomultiplier tube detector.

After filling 10 mM H_2O_2 and ECL solution to both microchannels of the BPE, PssRED and NssRED are respectively attached. The resulting ECL intensities were measured with a microscope (Nikon TE2000U) connected to a PMT detector (H10722-20, Hamamatsu) for 10 minutes. The obtained signals were analyzed using a self-programmed LabVIEW (LabVIEW 2015, National Instruments) program.

2.2.7. Fabrication of polyelectrolyte ionic diode and measurement of fluorescence

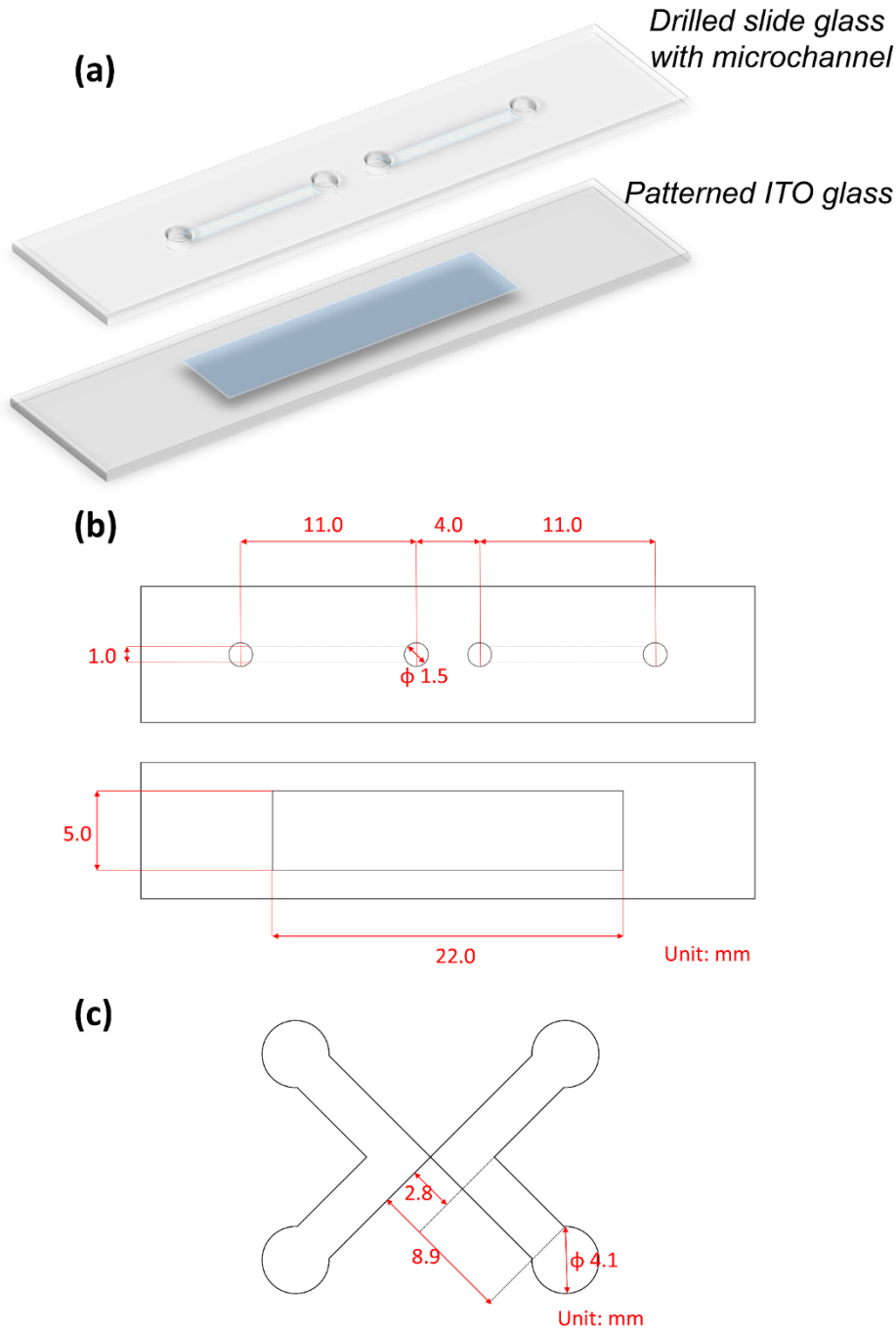

Figure 2-S1. (a) Schematic diagram of microchip for bipolar electrochemical

analysis. (b) Dimensions of the upper and bottom glass slides of BPE. In the upper glass, 50 μm deep microchannel was etched and the inlet was drilled. For the bottom glass, indium tin oxide bipolar electrode of 5.0 mm × 22.0 mm dimensions was etched. These two glasses were attached by thermal bonding. (c) Dimensions of X-shaped diode chip glass slide. 40 μm deep microchannel was etched.

X-shaped diode chips were prepared by previously reported procedures with dimensions shown in **Figure 2-S1**.[22] Fluorescein (1.7 μM in 0.1 M aqueous KCl) was loaded to both channels. 30-stack PssRED was directly attached to the channel openings of the X-shaped diode chips. The sign of bias was controlled by the direction of attachment. Fluorescence from the n-type polyelectrolyte gel was observed using a fluorescence microscope (TE2000U, Nikon, Japan).

2.3. Result and discussion

2.3.1. Strategies and design for solid salt REDs

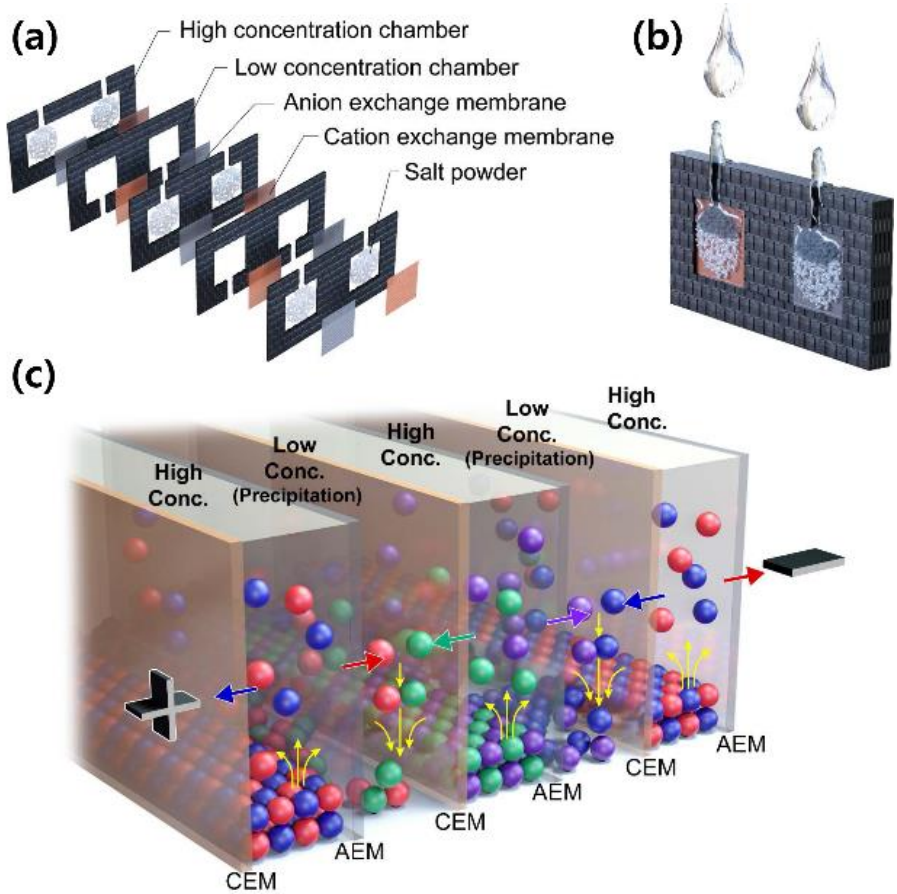

Figure 2-1. (a) Layered structure of the ssRED consisted of alternating HC and LC chambers. The outermost membranes constitute the interface with the target devices. (b) Schematic diagram of ssRED activation. Entry of water through inlets and dissolution of solid salts in high concentration chambers activate the ssRED. (c) Working principles of PssRED operation. **Figure 2-1** was reprinted from ref [41] Published by The Royal Society of Chemistry.

PssRED was strategically designed as follows. First, I envisioned to replace saline

solution with solid salt in the high concentration (HC) chamber to avoid the tedious injection processes (**Figure 2-1a**). I believed that, with this RED named solid salt RED (ssRED), the activation protocol could be simplified to a one-shot addition of small quantity of water (**Figure 2-1b**). Moreover, in terms of efficiency and economy, because the RED would stay dry prior to activation, it would be possible to be stored and distributed over longer time periods without any significant deterioration of performance. Secondly, ensuring that the ssRED maintains a prolonged steady state potential was of key importance. Therefore, to preserve low ionic concentrations in the LC chambers, I presented an unprecedented approach of introducing two different salts, which forms insoluble precipitates after ionic metathesis, alternatively into the HC chambers (**Figure 2-1c**). This type of ssRED is named precipitation-assisted ssRED (PssRED). Two kinds of ssRED are presented in this paper: one using only NaCl (NssRED) and other using $BaCl_2$ and Ag_2SO_4 (PssRED). The ssREDs are small (4.0 × 2.0 cm^2, thickness 250 μm/layer), comparable to a common universal serial bus (USB) flash drive and weigh only approximately 3 g (20 stack ssRED).

The theoretical verification of PssREDs is described as following. Two kinds of salts, $BaCl_2$ and Ag_2SO_4, are placed alternatively in HC chambers, then they are dissolved and ionized after the activation. Their solubility (maximum mass (g) of solute dissolvable in 100 mL of water) is 37 and 0.84, respectively.[38] The cations and anions in the HC chambers diffuse in opposite directions, forming barium sulfate ($BaSO_4$) and silver chloride (AgCl) by ionic metathesis in the LC chambers. These salts are insoluble as solubility products in water are 1.1×10^{-10} and 1.8×10^{-10}, respectively.[39] Therefore, precipitation keeps the concentration of LC chamber low so that the salinity ratio of each ion between HC and LC chambers in open circuit should be 1.64×10^5, 2.81×10^5, 4.21×10^3 and 2.54×10^3, for Ba^{2+}, Cl^-, Ag^+ and SO_4^{2-},

respectively.

2.3.2. Performance evaluation of ssREDs

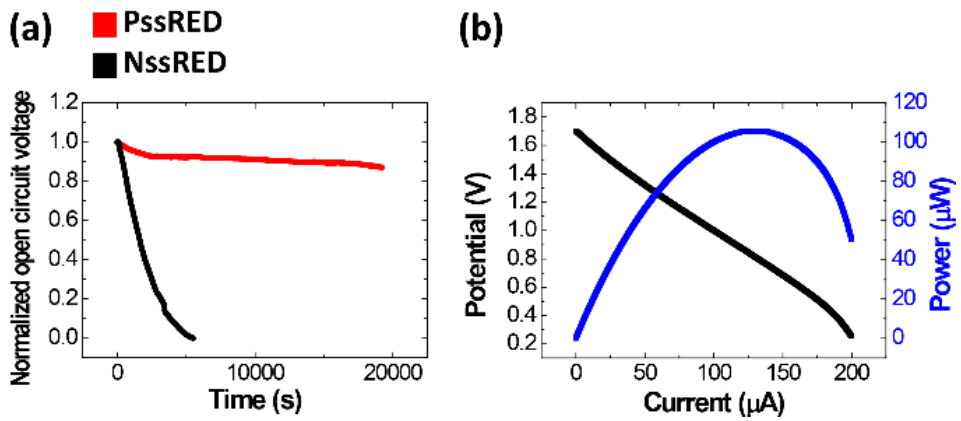

Figure 2-2. (a) Normalized open circuit potential (OCP)–time curve of 4-stack PssRED (red) and normalized OCP–time curve of NssRED (black). (b) Power (blue) and potential (black) curve of 20-stack PssRED versus operation current. **Figure 2-2** was reprinted from ref [41] Published by The Royal Society of Chemistry.

The performance evaluation of ssREDs as a power source is presented in **Figure 2-2**. I obtained the normalized time-dependent decay of open circuit potentials (OCP) to compare the durability of NssRED and PssRED. Reportedly, ion selectivity of the membranes is imperfect so that counterion transport reduces the concentration difference between HC and LC chambers, resulting in the rapid degradation of OCP.[40] However, the rate of decay is significantly lowered when the precipitation reaction take place in the LC chamber: OCP of NssRED rapidly decreases to 50% after 1500 s and completely diminishes after 5000 s, while that of PssRED decreases only marginally, preserving 90% of the maximum OCP even after 19000 s. This

clearly shows that precipitation reactions suppress the concentration building up in the LC chamber as expected.

As demonstrated in the current-potential curve shown in **Figure 2-2b**, the maximum power of a 20-stack PssRED is approximately 100 μW. Although this value is much lower than that required for devices that consume large electricity, it is enough to operate small devices like microfluidic ionic circuits.

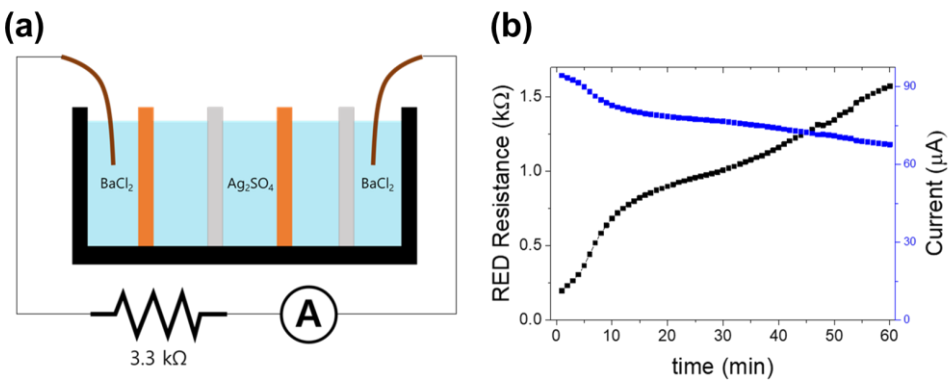

Figure 2-3. (a) 4-stack PssRED connected with resistor. (b) Time dependent RED resistance and current.

Theoretically, the RED would cease to function when the initial salt input is consumed to equal the concentrations in the LC chamber. Solely for a single saturated $BaCl_2$ chamber, the RED could run for 476 h at 100 μA condition (maximum power density condition). However, in reality, the chambers slowly dry over time due to water evaporation which provides the main reason of RED breakdown. The water loss is more severe in the LC chambers due to osmotic flow of water from the LC chamber to the HC chamber. Membrane clogging by precipitates is another issue that could reduce the performance of PssRED. These two issues, drying and membrane clogging, would cause the increase in internal

resistance of PssRED, reducing the cross-section area of the solution in the chambers. The internal resistance of PssRED was measured with the following scheme. As shown in **Figure 2-3a** 4-stack PssRED is prepared and the 3.3 kΩ resistor was connected via Ag/AgCl wire. 4-stack PssRED generates 0.32 V of OCP. When the resistor was connected, the battery operated with decreasing current. The internal resistance of a 4-stack PssRED is calculated from measured current (constant OCP was assumed), which increased from 198 to 1500 Ω in an hour. (**Figure 2-3b**) However, the value is insignificant considering the resistance of BPE microchip (hundreds of kΩ).

The charge that can be delivered by PssRED would be proportional to the initial salt loading. With the same setup which had been used to obtain the internal resistance of RED, total charge was measured until the PssRED was completely discharged. 1, 3, 10, 30 mg of $BaCl_2$ salt and the same number of moles of Ag_2SO_4 salt were loaded, which is 1.5 times in mass. In this experiment, the solutions in HC chambers are not saturated because the experiment time would be too long when the solution is saturated. Water was refilled every couple of hour during the measurement. As the result shown below in **Figure 2-4**, the delivered charge has linear relationship to the amount of $BaCl_2$ salt, although a large deviation from the theoretical charge (0.93 C / 1 mg of $BaCl_2$) was observed.

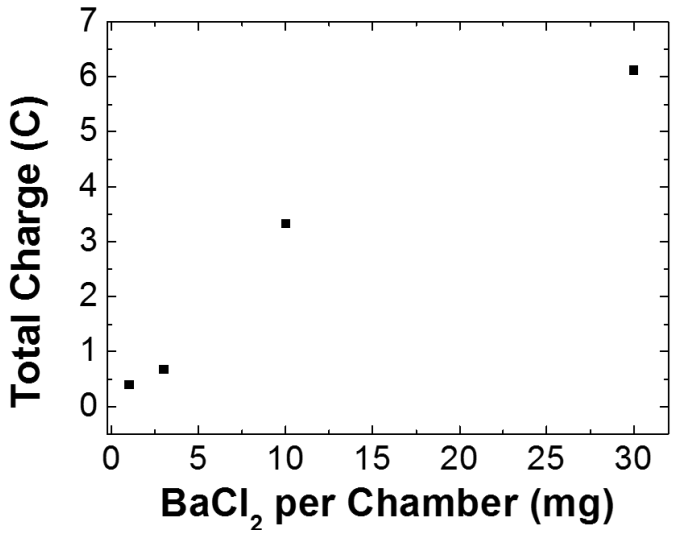

Figure 2-4. Total charge versus $BaCl_2$ per chamber in PssRED.

2.3.3. BPE sensing systems powered by ssREDs

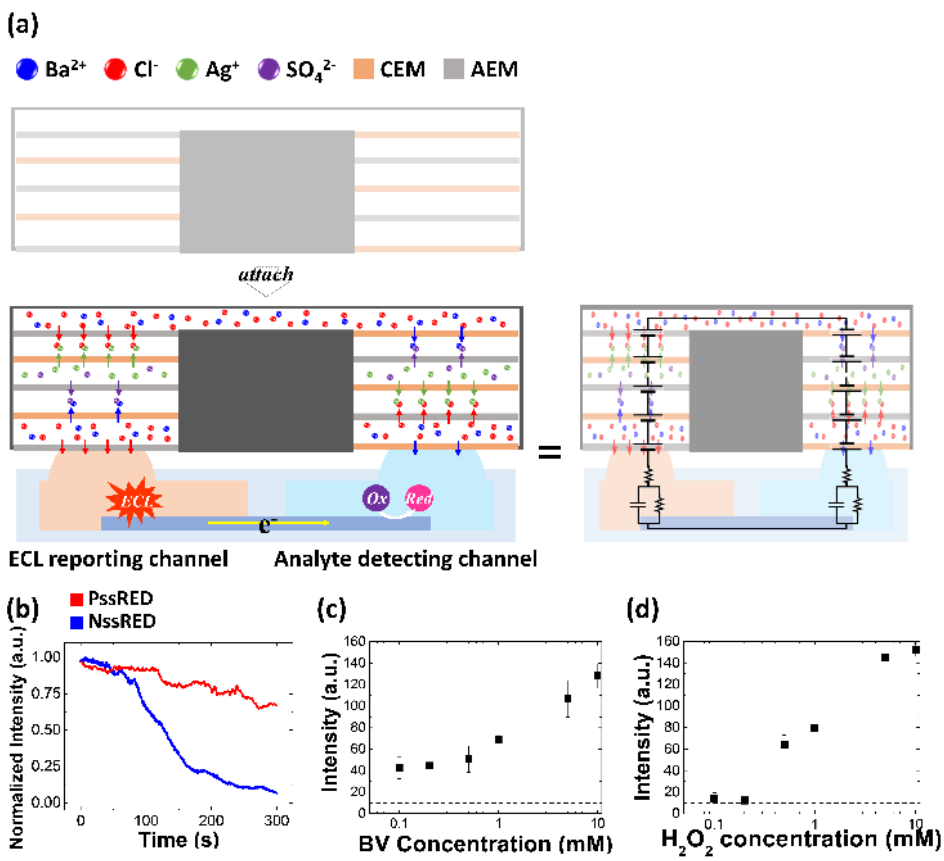

Figure 2-5. (a) Schematic diagram (left) and equivalent circuit (right) of RED powered BPE sensing chip. PssRED is placed on ITO-BPE microchip without any metallic contact. (b) Normalized ECL intensity over time using BPE chip powered by PssRED (red) and NssRED (blue). Analyte was 10 mM solution of H_2O_2 in PBS (pH 6.9). ECL intensity versus the concentration of (c) BV and (d) H_2O_2 using 30-stack PssRED powered BPE chip. Reporting channel: 5 mM $Ru(bpy)_3Cl_2$ and 25 mM TPA. Detecting channel: 0.2–10 mM BV and H_2O_2. All the solutions were made in pH 6.9 PBS. **Figure 2-5** was reprinted from ref [41] Published by The Royal Society of Chemistry.

To see if PssRED could successfully work as a new type of power source for low power devices, I conducted a series of experiments using an RED-powered BPE sensing platform (**Figure 2-5a**). This bipolar system consists of microchannels and an indium tin oxide (ITO) electrode lying underneath. The detecting and reporting channels are separated to prevent mutual interference. The ECL signal coupled with the reduction of model analysts, benzyl viologen and hydrogen peroxide, could be detected either by a digital camera or the naked eye. Quantitative analysis was performed by using the 30-stack PssRED-powered BPE sensing platform. For selection of the driving voltage, I performed individual cyclic voltammograms of aqueous 5 mM $Ru(bpy)_3^{2+}$-25 mM tripropylamine (TPrA), 1 mM BV, and 50 mM H_2O_2 solution, acquired on an ITO coated glass electrode against the Ag/AgCl reference electrode stored in 3 M NaCl solution.

In ECL process, excited $Ru(bpy)_3^{2+}$* is formed, which rapidly relaxes to the ground state, generating orange ECL signals at 630 nm at the potential higher than 0.9 V

(Blue curve in **Figure 2-6**). Moreover, BV^{2+} and H_2O_2 showed reduction onset potentials respectively at −0.4 V and −0.2 V (solid red and dashed red).

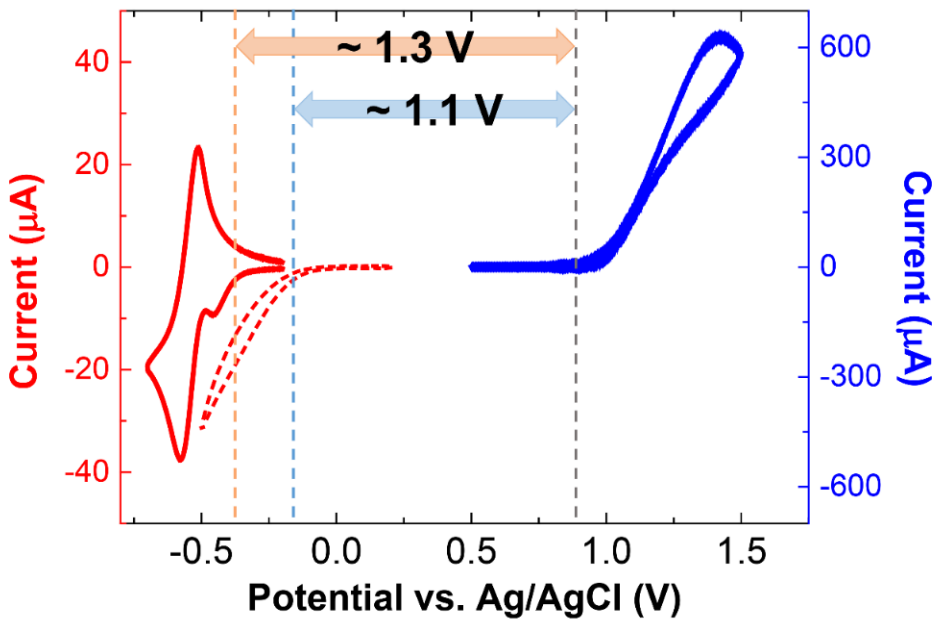

Figure 2-6. Cyclic voltammograms of 1 mM benzyl viologen (solid red), 50 mM hydrogen peroxide (dashed red) and 5 mM tris(2,2'-bipyridyl)dichlororuthenium(II) hexahydrate with 25 mM tripropylamine solution (blue). All the solutions were made in pH 6.9 PBS. Potential required for bipolar electrochemical analysis was 1.3 V and 1.1 V for benzyl viologen and hydrogen peroxide, respectively. **Figure 2-6** was reprinted from ref [41] Published by The Royal Society of Chemistry.

Therefore, the cyclic voltammograms show that the minimum potential for bipolar-ECL detection of the analytes is ~1.3 V and ~1.1 V for BV and H_2O_2, respectively. The necessary potential difference at driving electrodes could be calculated from equation 1, where ΔE_{elec} is effective potential difference, ΔE_{tot} is potential difference at driving electrodes, l_{elec} is BPE length and $l_{channel}$ is channel length.

$\Delta E_{elec} = \Delta E_{tot} \times (l_{elec}/l_{channel})$ (1)

Using the values, l_{elec} (=1.65 cm) and $l_{channel}$ (=1.90 cm), the calculation provided the necessary ΔE_{tot} as ~1.5V and ~1.3V respectively for BV and H_2O_2. In order to facilitate overcoming the overpotential and obtaining a detectable intensity of ECL, a practical value of 2.3 V was chosen (ΔE_{elec}=2.0 V).

As soon as direct contact between the BPE cell and the PssRED was made, ECL emission was observed at the anode of the BPE. First, I investigated the durability of ECL intensity because persistent ECL emission is crucial for consistent detection. It was measured using a homemade ECL analyzer consisted of a microscope and a photomultiplier tube (PMT). The ECL emission powered by PssRED was constant for the first 100 s and lasted for 300 s with intensity decreasing to merely ca. 70% of its initial value, while the ECL from NssRED-powered BPE started to diminish immediately, decreasing to ca. 70% of its initial value in 100 s (**Figure 2-5b**). The slight decrease of PssRED-powered ECL emission is not due to the power drop of the PssRED as the OCP of PssRED recovered fully after the measurement.

Next, calibration curves were constructed with a digital camera as the detector to take into account the actual environment where high-end instrument is not affordable (**Figure 2-5c** and **Figure 2-5d**). ECL emission was observed as soon as the direct contact between PssRED and BPE cell was made (**Figure 2-7**).

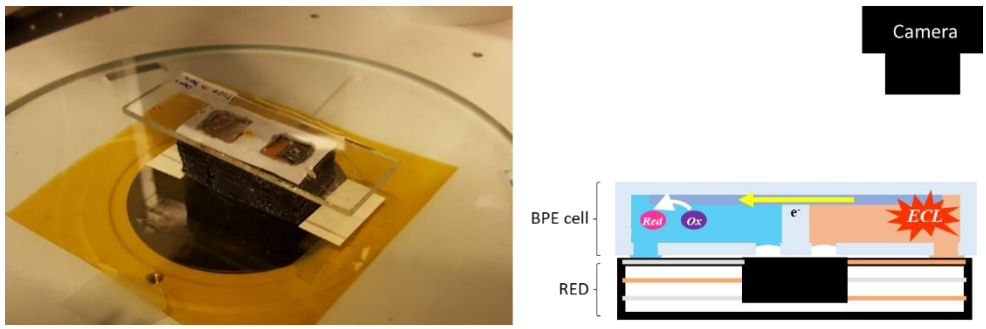

Figure 2-7. Photograph and schematic diagram of PssRED in contact with ECL sensing system.

Owing to its stability and durability, a single PssRED could run more than twenty BPE-ECL analysis once it is activated, even though each measurement took approximately 15 s. The whole calibration curve, hence, could be obtained with a single PssRED. Overall, PssRED powered BPE sensing platform showed analytical performance comparable to that powered by a potentiostat (**Figure 2-8**), corroborating that PssRED is an effective power source for small sensing devices.

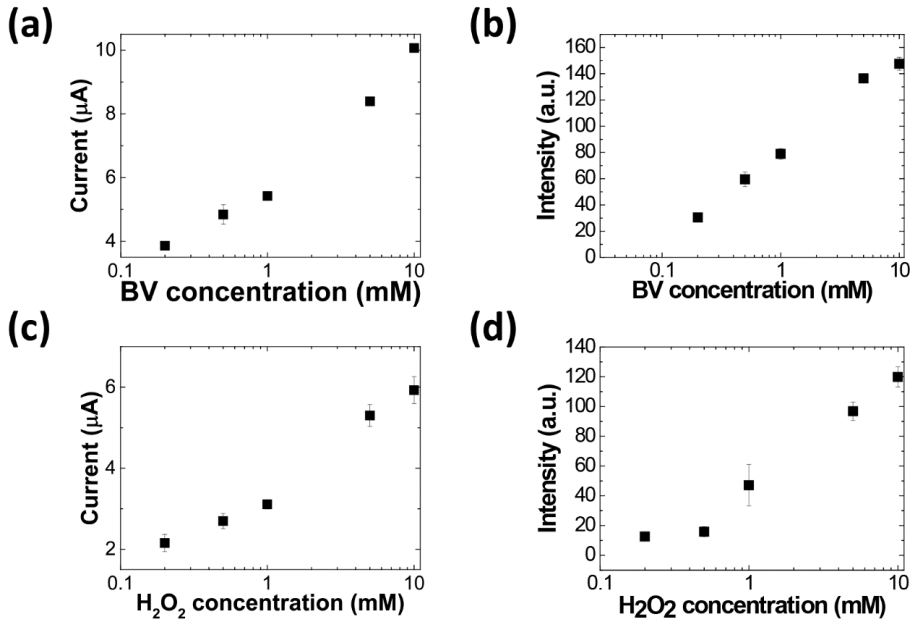

Figure 2-8. Current sampled 15 seconds after bias and ECL intensity of bipolar electrochemical system with varying the concentration of analytes. Bias of 2.3 V was applied by commercial potentiostat (Compactstat, Ivium). Reporting channel: 5 mM $Ru(bpy)_3Cl_2$ and 25 mM TPA. (a, b) Detecting channel: 0–10 mM BV. (c, d) Detecting channel: 0–10 mM H_2O_2. Applied potential is 2.3V. All the solutions were made in pH 6.9 phosphate buffer solution. **Figure 2-8** was reprinted from ref [41] Published by The Royal Society of Chemistry.

2.3.4. Polyelectrolyte ionic diodes powered by ssREDs

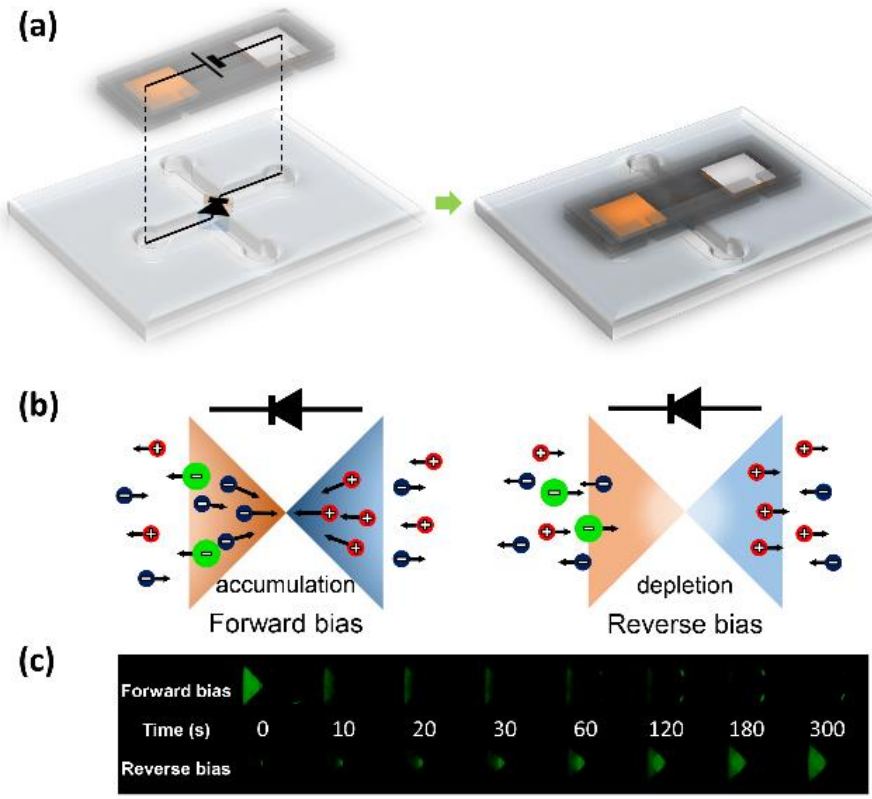

Figure 2-9. (a) Equivalent circuit and schematic diagram of polyelectrolyte ionic diode powered by PssRED. (b) Working principle of polyelectrolyte ionic diode system under each bias. (c) Temporal fluorescence images of the n-type polyelectrolyte gel (Forward bias: upper row, Reverse bias: lower row). **Figure 2-9** was reprinted from ref [41] Published by The Royal Society of Chemistry.

Finally, to confirm the possibilities of operating an ionic circuit with the PssRED system, the polyelectrolyte ionic diode previously reported by our group[7,22] was driven with a 30-stack PssRED. **Figure 2-9a** depicts the equivalent circuit and the direct attachment of the PssRED to the X-shaped polyelectrolyte ionic diode. In the

polyelectrolyte ionic diode system shown in **Figure 2-9b**, the counterions build up in the junction under forward bias, but dissipate to the bulk solution under reverse bias. Since the mobility of Cl^- is much larger than that of fluorescein (shown as green anions in the **Figure 2-9b**), it would push fluorescein against the electric field. Thus, under forward bias, fluorescein is driven out of the gel due to the influx of Cl^- ions, and vice versa under reverse bias. **Figure 2-9c** shows the temporal fluorescence measurements of the X-shaped diodes containing fluorescein solutions as the electrolyte. Fluorescence diminished over time under forward bias and intensified under reverse bias, confirming that the fully ionic circuit composed of ionic diodes and an ionic power source is successfully operating. This serves as an example to actually prove the capacity of PssREDs in driving ion-based systems, which eventually allow them to expand onto other biomimetic devices.

2.4. Conclusion

In this work, I proposed a new concept of battery that functions without any metallic components or other solid conducting materials. It is based on the working principle of RED where the salinity gradient is transduced to electricity. The use of a pump, a necessary component to maintain constant electricity but a critical drawback for miniaturization, is removed by employing a pair of dry salt. When an RED contains dry salt in HC chambers, it can be easily activated by simply immersing in water. The stability and durability of ssRED were remarkably improved by using a pair of soluble salts that can form insoluble salts by exchanging their counterions (PssRED). Precipitation reactions in LC chambers maintain low concentrations so that electromotive force is rendered stable for several hours. PssRED can supply

consistent power to run small devices, demonstrated through driving the bipolar-ECL sensor apparatus and the polyelectrolyte ionic diode. Furthermore, the operating voltage could be customized for target usage by adjusting the number of stacks. I believe that the PssRED exhibits exceptional prospect for applications to a wide range of ion-based platforms such as bio-interfacing and drug delivery, and further investigation is ongoing in our laboratory.

2.5. References

(1) B. Lovrecek, A. Despic and J. O. M. Bockris, *J. Phys. Chem.*, 1959, **63**, 750.

(2) O. J. Cayre, S. T. Chang and O. D. Velev, *J. Am. Chem. Soc.*, 2007, **129**, 10801.

(3) E. O. Gabrielsson, P. Janson, K. Tybrandt, D. T. Simon and M. Berggren, *Adv. Mater.*, 2014, **26**, 5143.

(4) K. Tybrandt, E. O. Gabrielsson and M. Berggren, *J. Am. Chem. Soc.*, 2011, **133**, 10141.

(5) K. Tybrandt, K. C. Larsson, A. Richter-Dahlfors and M. Berggren, *Proc. Natl. Acad. Sci.*, 2010, **107**, 9929.

(6) K. Tybrandt, R. Forchheimer and M. Berggren, *Nat. Commun.*, 2012, **3**, 871.

7. J.-H. Han, K. B. Kim, H. C. Kim and T. D. Chung, *Angew. Chem. Int. Ed.*, 2009, **48**, 3830.

(8) H. Sun, M. Vagin, S. Wang, X. Crispin, R. Forchheimer, M. Berggren and S. Fabiano, *Adv. Mater.*, 2018, **30**, 1704916.

(9) P. Ramirez, J. Cervera, M. Ali, W. Ensinger and S. Mafe, *ChemElectroChem*, 2014, **1**, 698–705.

(10) C. J. Wan, L. Q. Zhu, J. M. Zhou, Y. Shi and Q. Wan, *Nanoscale*, 2013, **5**, 10194.

(11) Y. Li, M. Wu, D. Zhao, Z. Wei, W. Zhong, X. Wang, Z. Liang and Z. Li, *Sci. Rep.*, 2016, **5**, 17817.

(12) M. Grys, Z. Madeja and W. Korohoda, *Cell. Mol. Biol. Lett.*, 2017, **22**, 1.

(13) B. Taji, S. Shirmohammadi, V. Groza and I. Batkin, *IEEE Trans. Instrum. Meas.*, 2014, **63**, 1412.

(14) P. F. Meyer, P. D. Gadsby, D. Van Sickle, W. E. Schoenlein, K. S. Foster and G. P. Graber, *Med. Biol. Eng. Comput.*, 2005, **43**, 225.

(15) S. E. Fosdick, K. N. Knust, K. Scida and R. M. Crooks, *Angew. Chem. Int. Ed.*, 2013, **52**, 10438.

(16) C. Wang, K. (Kelvin) Fu, J. Dai, S. D. Lacey, Y. Yao, G. Pastel, L. Xu, J. Zhang and L. Hu, *Nat. Commun.*, 2017, **8**, 15609.

(17) R. E. Pattle, *Nature*, 1954, **174**, 660.

(18) B. E. Logan and M. Elimelech, *Nature*, 2012, **488**, 313.

(19) M. Tedesco, A. Cipollina, A. Tamburini and G. Micale, *J. Memb. Sci.*, 2017, **522**, 226.

(20) J. G. Hong, B. Zhang, S. Glabman, N. Uzal, X. Dou, H. Zhang, X. Wei and Y. Chen, *J. Memb. Sci.*, 2015, **486**, 71.

(21) X. Tong, B. Zhang and Y. Chen, *J. Memb. Sci.*, 2016, **516**, 162.

(22) S. H. Han, S.-R. Kwon, S. Baek and T.-D. Chung, *Sci. Rep.*, 2017, **7**, 14068.

(23) S.-R. Kwon, S. H. Nam, C. Y. Park, S. Baek, J. Jang, X. Che, S. H. Kwak, Y.-R. Choi, N.-R. Park, J.-Y. Choi, Y. Lee and T. D. Chung, *Adv. Funct. Mater.*, 2018, 1705952.

(24) S. Baek, S.-R. Kwon, S. Y. Yeon, S.-H. Yoon, C. M. Kang, S. H. Han, D. Lee and T. D. Chung, *Anal. Chem.*, 2018, **90**, 4749.

(25) W. Zhan, J. Alvarez and R. M. Crooks, *Anal. Chem.*, 2003, **75**, 313.

(26) B.-Y. Chang, K.-F. Chow, J. A. Crooks, F. Mavré and R. M. Crooks, *Analyst*, 2012, **137**, 2827.

(27) W.-X. Lu, N. Bao and S.-N. Ding, *RSC Adv.*, 2016, **6**, 25388–25392.

(28) M.-S. Wu, D.-J. Yuan, J.-J. Xu and H.-Y. Chen, *Chem. Sci.*, 2013, **4**, 1182.

(29) F. Mavré, R. K. Anand, D. R. Laws, K.-F. Chow, B.-Y. Chang, J. A. Crooks and R. M. Crooks, *Anal. Chem.*, 2010, **82**, 8766.

(30) W. Zhan, J. Alvarez and R. M. Crooks, *J. Am. Chem. Soc.*, 2002, **124**, 13265.

(31) A. L. de Lacey, M. T. Bes, C. Gómez-Moreno and V. M. Fernández, *J. Electroanal. Chem.*, 1995, **390**, 69.

(32) C. L. Bird and A. T. Kuhn, *Chem. Soc. Rev.*, 1981, **10**, 49.

(33) N. Nasirizadeh, Z. Shekari, A. Nazari and M. Tabatabaee, *J. Food Drug Anal.*, 2016, **24**, 72.

(34) A. Noorbakhsh, M. Khakpoor, M. Rafieniya, E. Sharifi and M. Mehrasa, *Electroanalysis*, 2017, **29**, 1113.

(35) L. Wang, *Electrochem. Commun.*, 2004, **6**, 225.

(36) S. Z. Bas, C. Cummins, D. Borah, M. Ozmen and M. A. Morris, *Anal. Chem.*, 2018, **90**, 1122.

(37) H. Chun and T. D. Chung, *Annu. Rev. Anal. Chem.*, 2015, **8**, 441.

(38) D. R. Lide, *CRC Handbook of Chemistry and Physics*, CRC Press, Boca Raton, FL, USA 2003.

(39) A. E. Martell and R. M. Smith, *Critical stability constants. 4. Inorganic complexes*, Plenum Press, New York, NY, USA 1976.

(40) T. Sata, *J. Memb. Sci.*, 1994, **93**, 117.

(41) S. Y. Yeon, J. Yun, S, Yoon, D. Lee, W. Jang, S. H. Han, C. M. Kang, T. D. Chung, *Chem. Sci.* 2018, **9**, 8071-8076.

Chapter 3. Development of paper based electrochromic glucose sensor

Parts of this chapter were published as S. Y. Yeon[1]; M. Seo[1]; Y. Kim; H. Hong; T. D. Chung*. "Paper-based electrochromic glucose sensor with polyaniline on indium tin oxide nanoparticle layer as the optical readout" *Biosens. Bioelectron.* **2022**, 203, 114002. S. Y. Yeon, M. Seo and T. D. Chung conceived the concept and designed the experiments. S. Y. Yeon. and M. Seo carried out the experiments.

3.1. Introduction

With the increasing demands of point-of-care (POC) testing in diagnostic analysis, various studies have been conducted to develop portable, flexible, low cost, and easy-to-use sensors.[1,2] Being light and eco-friendly, paper has been extensively utilized as the material of choice for cost-effective sensor platforms.[3–7] In particular, since the demonstration by Whitesides,[8–12] numerous studies on the development of paper-based electrodes as an alternative to traditional electrochemical sensors have been reported in regard to field diagnosis concerning environmental and health issues. Meanwhile, applying colorimetric detection in sensors exhibit great merit when used by unskilled users as data can be easily interpreted with the naked eye without the need of external readout devices. Accordingly, colorimetric tests have been regarded as useful detection methods for paper-based sensor devices. However, conventional colorimetric systems based on enzymatic reactions coupled with redox indicators suffer from long response time, difficulty in material recycling, and lack of color homogeneity due to the diffusion of colorimetric compounds.[13–15] Moreover, precise quantitative analysis is challenging, as monochromatic systems mandate additional analytic devices.[16–18]

In this regard, paper-based electrochemical sensors combined with electrochromic materials as optical reporters offer many advantages such as fast switching time, re-usability, and color uniformity.[17–20] However, as colorimetric detections require transparent or light-colored backgrounds, the choice of electrode substrates for electrochromic indicator immobilization are limited to materials such as indium tin oxides (ITO)[17,21,22] or metals.[23,24] As ITO films are traditionally fabricated by sputtering,[25] thermal evaporation[26] or sol-gel methods[27] that involve annealing

procedures at high temperatures (T≥300 ℃), the fabrication of electrochromic sensors built entirely on paper have been challenging, requiring the introduction of ITO/glass substrates[17,22] While several studies have reported colorimetric readout devices on flexible substrates by means of coating gold metals,[23,28,29] the high cost would limit the development of disposable or large-scale devices.

Recently, motivated by the demands for flexible optoelectronic devices (OLEDs, touch-panel displays) and solar cells, various low-temperatures deposition methods of ITO on flexible substrates have been developed, including vapor deposition[30–32] and nanoparticle coating methods.[33,34] Fabrication of ITO films in the form of ITO nanoparticles is particularly effective in obtaining light-colored substrates, even when deposited upon carbon-based electrodes.[35,36] A few studies have integrated electrochromic materials with carbon-based electrodes so far, one of which is the recent work of Aller-Pellitero et al., where Prussian Blue (PB)-modified ITO or SiO_2-ATO particles were deposited on graphite screen-printed electrodes, enabling the electrochemical, as well as colorimetric detection of hydrogen peroxide and glucose.[36] Given the many advantages of carbon-based electrodes, including low cost, good conductivity and ease in fabrication[6], rendering it applicable as substrates for electrochromic signal display will open up new opportunities towards paper-based electrochromic sensors. However, despite the introduction of low-temperature processes of ITO film deposition, electrochromic sensors reported so far have rarely employed paper as the substrate, and even in that case, non-flexible ITO substrates have been added for the deposition of electrochromic materials.[17,37]

Herein, we present an electrochemical sensor built entirely on a single paper substrate that enable visual detection of analytes through the variation of colors. The formation of ITO particle layers on the screen-printed carbon produced a conductive

and light-colored film on the paper substrate, allowing electrodeposition of electrochromic materials. Upon deposition of polyaniline (PANi), an electrochromic indicator, on the ITO particle layer, colorimetric signals could be perceived with little interference from the underlying carbon electrode. We demonstrated that the change in the concentration of analytes (hydrogen peroxide and glucose) could be displayed by the color shift of polyaniline. As polyaniline is well known for its wide range of colors (yellow, green, blue, and purple), it provides a convenient colorimetric readout for distinguishing the amount of analyte. Furthermore, the glucose concentration could be quantified based on the hue values of polyaniline. Through this work, we have established a colorimetric sensor system that utilizes the advantages of both electrochemical sensing and colorimetric readout, demonstrating feasible analyte detection with reduced time and cost.

3.2. Experimental

3.2.1. Materials

Cetyl trimethyl ammonium bromide (CTAB), iron (III) chloride ($FeCl_3$), potassium ferricyanide (III) ($K_3Fe(CN)_6$), potassium chlo-ride (KCl), potassium phosphate dibasic, potassium phosphate monobasic, aniline, glucose oxidase (GOx), bovine serum albumin, chitosan, glucose, glutaraldehyde were purchased from Sigma Aldrich (St. Louis, Missouri, U.S.A.), hydrogen peroxide (H_2O_2) were purchased from Samchun Chemicals (South Korea), all of which were used without further purification. All aqueous solutions in this experiment were prepared with ultrapure deionized water (resistivity ~18.2 MΩ) produced by NANO pure Diamond (Barnstead, New Hampshire, U.S.A.). ITO nanoparticle powder (20-70 nm diameter)

was purchased from US Research Nanomaterials, and carbon/graphite screen-printing paste from Gwent. Filter paper (grade 2) was purchased from Whatman (Maidstone, Kent, U.K.).

All electrochemical measurements in this work were done using a potentiostat (CHI 660, CH Instruments). The morphology of the ITO modified carbon electrodes were observed with a Field-Emission Scanning Electron Microscope (S-4300, Hitachi). The sheet resistances of the electrodes were measured using a 4-point probe (FPP-5000, Changmin).

3.2.2. Fabrication of ITO modified carbon electrodes

The carbon/graphite screen printing paste was first diluted with a mixture of acetone and cyclohexanone (1:1 in weight) to obtain moderate viscosity for the screen-printing process. Then, the carbon paste was applied on a filter paper substrate (Whatman, grade 2) using a silk screen template to form the working and counter electrodes, each with a dimension of 1 cm × 4.5 cm (supplementary figure 1). The screen printing process was repeated 3-4 times until carbon electrodes with sufficient conductivity was achieved. The pseudo-reference electrode was printed on the same paper substrate by applying silver/silver chloride ink (ALS) followed by heat treatment on a 150 ℃ hot plate for 30 mins.

For the purpose of colorimetric detection, ITO nanoparticle films were deposited on one of the carbon electrodes, producing ITO modified carbon electrodes. In this step, the ITO slurry was first prepared by combining ITO nanoparticle dispersion (30 wt% in ethanol) and Mowiol 4-88 (12 wt% in water) with 6:4 volume ratio. The ITO was deposited on the counter carbon electrode by spin coating the ITO slurry on the

partially exposed carbon electrode substrate. Afterwards, the ITO films were cured with UV light for 15 mins to increase the conductivity.[34] The spin coating and the subsequent UV exposure steps were repeated multiple times to obtain moderately thick ITO films with sufficiently light-colored backgrounds for their use in colorimetry. To further improve the conductivity of ITO films, the electrodes were then annealed in forming gas (5% H_2/N_2) at 130 °C for 1 h (Thermal CVD System, SciEnTech).

Finally, electrochromic polyaniline (PANi) was electrodeposited on the ITO modified carbon electrode by applying a constant voltage of 0.9 V (vs Ag/AgCl) in 0.5 M aniline / 1.0 M H_2SO_4 solution until the total charge reached 0.2 C/cm^2. For the observation of electrochromic properties of Prussian blue (PB), electrodeposition was made by immersing the ITO modified carbon electrode in 20 mM $FeCl_3$ and 20 mM $K_3Fe(CN)_6$ in 0.1 M KCl solution containing 0.02 M HCl, and a current of 30 μA/cm^2 was passed for 60s.

3.3.3. Modifications of electrodes for analyte sensing

Prussian blue (PB) was first introduced on the working carbon electrode for the detection of H_2O_2. First, 0.92 mM CTAB, 0.5 mM $FeCl_3$ and 0.5 mM $K_3Fe(CN)_6$ in 0.1 M KCl solution containing 0.02 M HCl were prepared. The PB films were then electrodeposited on the carbon electrode via cyclic voltammetry (75 cycle, 100 mV/s).

To immobilize glucose oxidase on the PB-modified carbon electrode, 600 μL of GOx solution (40 mg/mL GOx, 10 mg/mL BSA) was drop cast on the electrode and dried for 1 h in room temperature. Afterwards, the electrode was covered with 1%

chitosan solution and dried for 2 h. Then the electrodes were soaked in 2.5% Glutaraldehyde solution for 5 mins and washed with PBS (pH 5.0). Finally, the GOx solution was drop cast again on the electrode and then dried.

3.3.4. Colorimetric detection of hydrogen peroxide and glucose

H_2O_2 analyte solutions were prepared with 0.1 M PBS (pH 3.0) as the electrolyte. With PB modified carbon electrode as the working electrode, and the PANi deposited ITO/carbon electrode as the counter electrode, the colorimetric signals of PANi according to H_2O_2 concentrations ranging from 2.5×10^{-4} to 5.0×10^{-3} M were obtained with an applied voltage of −0.2 V (vs Ag/AgCl paste reference electrode).

For the detection of glucose, solutions of glucose concentrations from 1.0×10^{-4} to 1.0×10^{-2} M in 0.1 M PBS (pH 5.0) were prepared. The colorimetric responses of PANi towards glucose concentration were obtained with applied potential of 0 V (vs Ag/AgCl paste reference electrode). Color images of PANi electrodes were acquired after 30 s. These measurements were performed with all three electrodes fabricated on the same paper substrate.

3.3.5. Hue value calculation

Photographs of PANi electrodes were analyzed using ImageJ software. The pixel values (R, G, B values) of the images were obtained as an average of all pixels. Among the three, the maximum value (max) and the minimum value (min) determined the hue values according to the equations below.[38]

If max = R, then hue value = 60 × ((G – B) ÷ (R – min))

If max = G, then hue value = 60 × (2.0 + (B – R) ÷ (G – min))

If max = B, then hue value = 60 × (4.0 + (R – G) ÷ (B – min))

3.3. Result and discussion

3.3.1. Characterization of ITO modified carbon electrodes

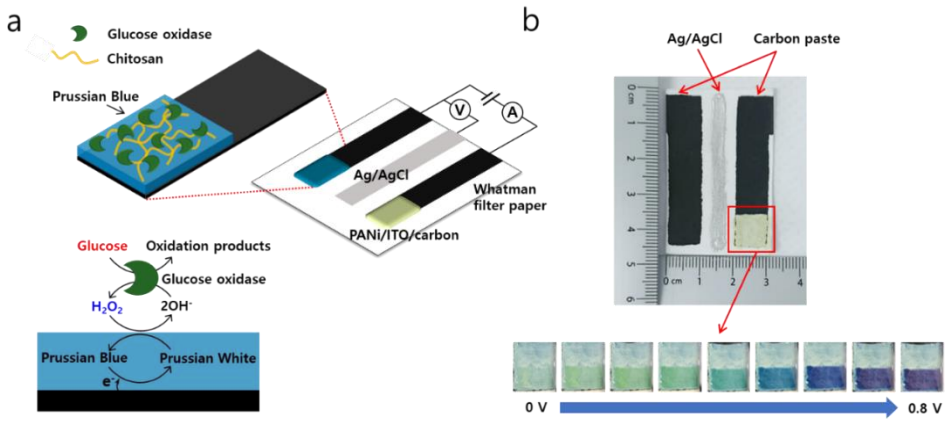

Figure 3-1. (a) The components of the paper based electrochromic sensor and the sensing principle of glucose (b) Photograph of the sensor showing (from left) the working, reference, and the counter electrode (before the deposition of PANi). The lower part displays the potential-dependent colors after the deposition of PANi.

Figure 3-1a outlines the components of the paper based electrochromic sensor, and its sensing principle. The sensor is comprised of a working electrode, counter electrode, and Ag/AgCl reference electrode, all of which are located on the same paper substrate. For efficient analyte reaction to take place, catalytically active material is introduced on the carbon working electrode. In this work, Prussian blue (PB) and glucose oxidase (GOx)/PB was employed for the detection of hydrogen peroxide and glucose, respectively. Colorimetric signals are displayed at the counter electrode, where the electrochromic material is deposited on ITO modified carbon

electrodes. When potential is applied to the working electrode (vs Ag/AgCl reference electrode), current generated from the analyte reaction alters the potential being applied on the counter electrode. Then, the potential-dependent electrochromic reactions occurring at the counter electrode enable the colorimetric detection of analytes.

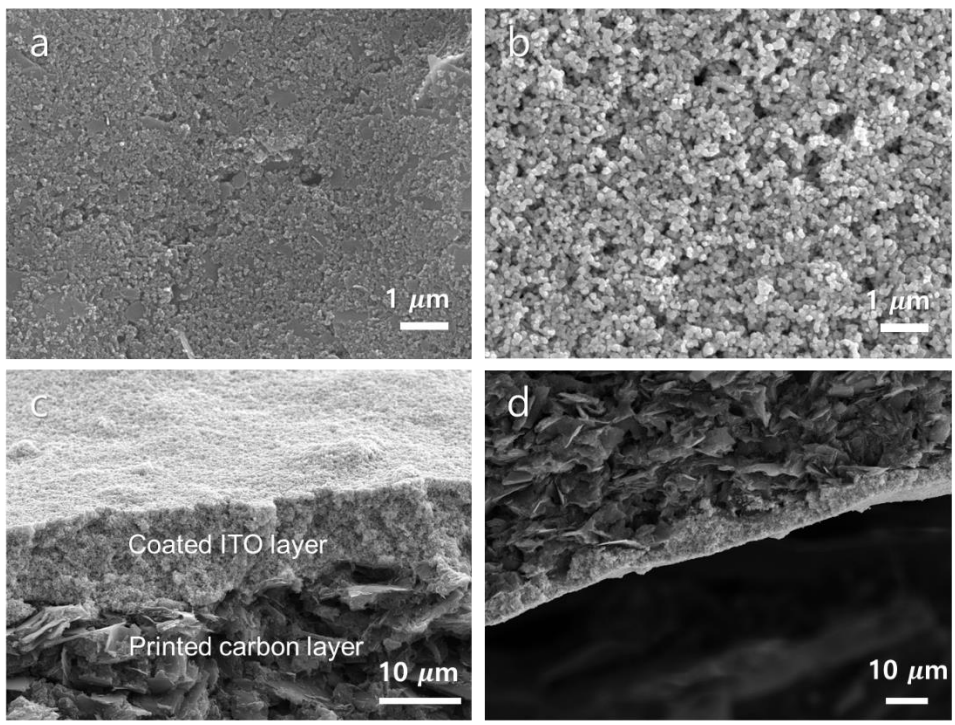

Figure 3-2. SEM images of ITO deposited carbon electrodes. (a) Top view of screen-printed carbon on the paper substrate. (b) Top view of ITO/carbon electrode. (c) Cross-section view of ITO/carbon electrode (d) Cross-section view of ITO/carbon electrode after bending the electrode.

For effective colorimetric signal readout, a substrate for the deposition of the electrochromic material was manufactured by modifying the counter electrode with ITO nanoparticle layers. The deposition of ITO nanoparticles on paper substrates

was performed by applying a low-temperature method introducing polymer based composites.[34] The polyvinyl alcohol (PVA)-ITO nanoparticle mixture was spin coated on the paper based carbon electrodes, forming ITO modified carbon electrodes (which we will refer as "ITO/carbon electrode"). The morphology of various ITO/carbon electrodes were observed with FESEM (**Figure 3-2**). **Figure 3-2a** and **2b** each represents the top view of the paper based carbon electrodes before and after spin coating ITO nanoparticles. Upon the deposition of ITO, nanoporous structures with random pores are formed. The cross section image of **figure 3-2c** show that the ITO nanoparticle layer is formed on the printed carbon. **Figure 3-2d** shows the cross section image of an ITO/carbon electrode after bending the substrate around a plastic tube with a radius of 20 mm. It can be seen that the ITO/carbon layer retains its structure, and is robust enough to be used as flexible substrates.

Furthermore, the color of the ITO/carbon electrodes could be optimized by tuning the ITO nanoparticle layer thickness. Upon increasing the number of spin coating process from 1 to 4 times, the porous ITO layer increased accordingly, forming ITO layers with no visible gaps between the processes. Also, the addition of ITO layers gradually shifts the substrate colors from grey to light. For the fabrication of colorimetric sensors introduced in the following section, ITO/carbon electrodes which were spin coated 3 times were used.

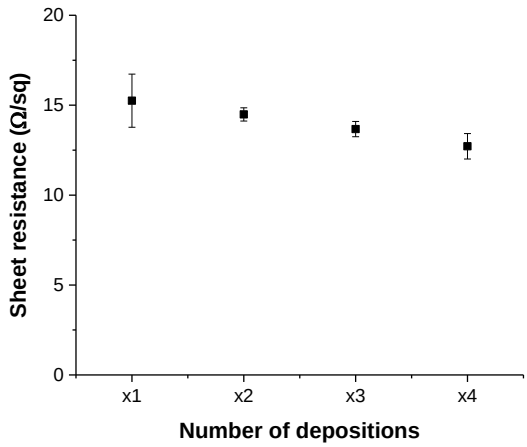

Figure 3-3. Sheet resistance of ITO modified carbon electrodes according to the number of spin-coated layers

The conductance of the ITO/carbon electrodes was also examined by 4-point probe measurements. The sheet resistance according to the number of spin-coated ITO layers is shown in **figure 3-3**, where the electrodes show adequately low resistance regardless of the ITO layer thickness, presumably due to the formation of a dense ITO-polymer network. Thus, the deposition of opaque, light yellow colored ITO nanoparticles yielded a conductive yet light-colored substrates despite the underlying carbon, providing a suitable substrate for colorimetric detection (**figure 3-1b**).

3.3.2. Colorimetric signals of PANi deposited on ITO modified carbon electrodes

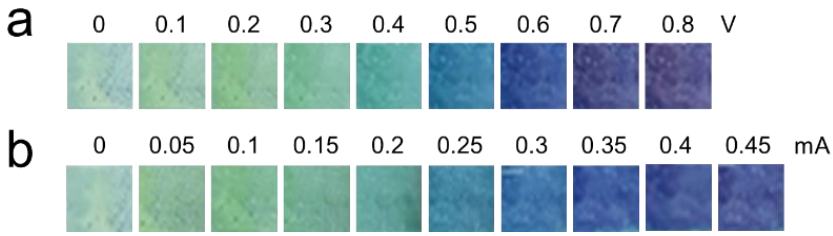

Figure 3-4. (a) Color responses to series of applied potentials, taken after 15 s. (b) Color responses to series of applied currents taken after 30 s.

Electrochromic Polyaniline (PANi) was electrodeposited on the ITO/carbon electrodes, yielding a "PANi/ITO/carbon electrode". Before demonstrating its application in colorimetric sensors, the colorimetric signals of PANi on the ITO/carbon electrodes were first characterized according to the applied potential or currents. First, the potential-dependent colorimetric signals of PANi/ITO/carbon electrode were observed upon applying potentials in the range of 0 to 0.8 V with an interval of 0.1 V. To gain a stable colorimetric signal, images were taken after the potentials were applied for 15 s. **Figure 3-4a** shows that as the applied potential becomes more positive, the PANi/ITO/carbon electrode displays a clear change from colorless to green, blue, and purple sequentially.

The current-dependent colorimetric signals of PANi/ITO/carbon electrodes were also observed by applying constant currents in the range of 0 to 0.45 mA with an interval of 0.05 mA. Images taken after applying currents for 30s are shown in **Figure 3-4b**. Similar to the potential-dependent colors of PANi, oxidative currents changed the PANi color from colorless to green, blue and purple, covering the full

color range of PANi. As the reducing current from the analyte reaction at the working electrode is equivalent to the oxidative current flowing through the counter electrode, the color shift of PANi-deposited counter electrode could be used to quantitatively detect the current at the working electrode. Thus, we set out to apply PANi for the detection of hydrogen peroxide and glucose, as described in the following section.

3.3.3. Colorimetric detection of hydrogen peroxide with Prussian blue/Carbon working electrodes

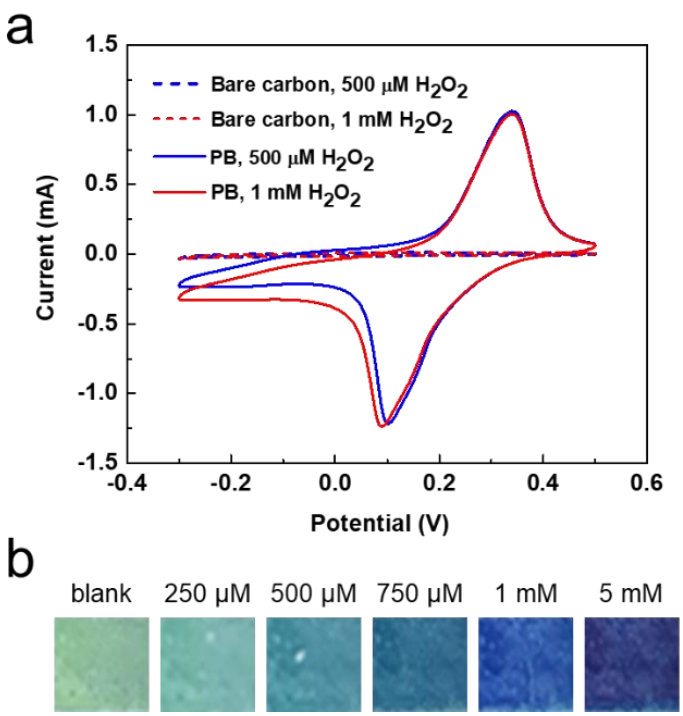

Figure 3-5. (a) Cyclic voltammogram of bare carbon electrode (dashed lines) and PB deposited carbon electrode (solid lines) with varying H_2O_2 concentration. (b) Colorimetric signals of PANi according to H_2O_2 concentration.

Based on the aforementioned sensing principle, colorimetric detection of hydrogen peroxide (H_2O_2), a representative byproduct generated from various enzymatic reactions, is demonstrated as a proof-of-concept. Prussian blue (PB), a representative catalyst towards H_2O_2, was utilized as the catalytic material and deposited on the carbon working electrode. Under an applied potential, PB is electrochemically reduced to Prussian white (PW), which in turn reduces hydrogen peroxide with good selectivity and sensitivity. The catalytic effect of PB/carbon electrode towards H_2O_2 is demonstrated by the cyclic voltammogram in **Figure 3-5a**, where increased reduction currents of the PB deposited carbon electrode compared to the bare carbon electrode can be seen. For the colorimetric detection of H_2O_2, a constant potential of −0.2 V (vs. printed Ag/AgCl) was applied on the working electrode, and the colorimetric signals of PANi with varying H_2O_2 concentrations were obtained after 30 s (**Figure 3-5b**). A clear change in color can be observed with increasing H_2O_2 concentration, with a distinguishable shift from yellow to dark blue in the range of a few hundreds of μM, finally showing a color between dark blue and purple at 5 mM. No noticeable color change was observed before applying the potential.

This demonstrates that, upon deposition of PB, a feasible electrochromic sensor towards hydrogen peroxide with PANi as the colorimetric readout can be achieved. As hydrogen peroxide is a byproduct of various metabolic enzymes (e.g., glucose oxidase), combination of PB with appropriate enzymes could effectively detect a wide range of analytes.

3.3.4. Colorimetric glucose sensor with GOx/PB/Carbon

working electrodes

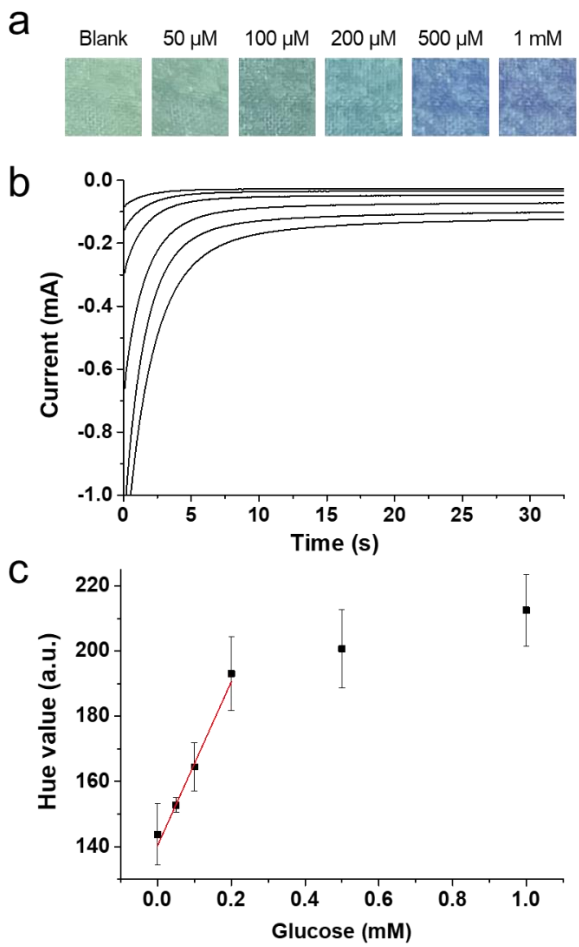

Figure 3-6. (a) Colorimetric signals of PANi/ITO/carbon electrodes according to the glucose concentration. (b) Chronoamperometric data obtained while applying constant potential for glucose concentrations of 0, 0.05, 0.1, 0.2, 0.5, and 1 mM (c) The hue values of PANi plotted against the glucose concentration, and the linear fit (red) for the glucose concentration from 0 to 0.2 mM is shown.

The versatility of the PANi based colorimetric sensor was further demonstrated by quantitatively analyzing glucose. For the selective detection of glucose, glucose

oxidase (GOx) was deposited on the previously demonstrated PB/carbon working electrode, yielding GOx/PB/carbon electrode. At this electrode, GOx oxidizes glucose in the analyte solution, producing H_2O_2 as the result of the enzymatic reaction. Consequently, PB reduces H_2O_2, of which the amount is in proportion with that of glucose (**Figure 3-1**). Therefore, the glucose concentration can be visualized by the electrochromic reaction at the counter electrode.

0 V (vs. printed Ag/AgCl) was chosen as the potential to be applied on the GOx/PB/carbon working electrode in order to obtain significant change in color with differing glucose concentration. At this potential, the reduction currents increased with the glucose concentration (**Figure 3-6b**), confirming the catalytic effect of GOx/PB/carbon electrode. The colorimetric signals of PANi according to the glucose concentration are displayed in **Figure 3-6a**. Distinguishable color change can be seen with the increase of glucose concentration, with the colors shifting from dark green to blue, finally reaching purple for 1 mM.

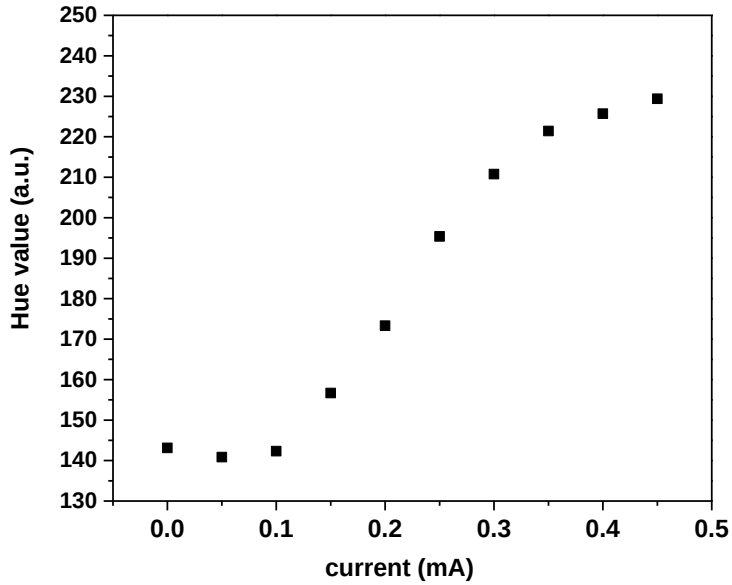

Figure 3-7. Hue values of PANi according to the applied current.

By converting each color to their hue values, the colorimetric signals could be further utilized for the quantitative measurement of glucose. Earlier, we had demonstrated the change in PANi colorimetric signals according to the current flow (**Figure 3-4b**). Plotting the hue values of each colorimetric signals against the corresponding current reveals a linear relationship when the hue value is in the range from 140 to 200 (**Figure 3-7**). Thus, the current flowing at the counter electrode, and therefore the current at the working electrode due to the glucose reduction could be determined if the hue values displayed at the counter electrode belong in this range. The calibration curve obtained for the glucose concentration and the corresponding hue values are shown in Figure 5c, and a linear fit of the hue values according to the glucose concentration is shown in the range of 0 mM to 0.2 mM glucose. The limit of detection value, calculated as the lowest analyte concentration with the signal three standard deviations above those of the blank solution, was 126 μM.

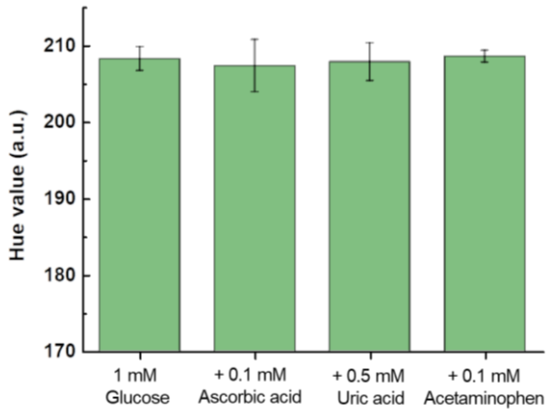

Figure 3-8. The hue values of PANi colorimetric signals of 1 mM glucose and after the addition of interfering species 0.1 mM ascorbic acid, 0.5 mM uric acid, and 0.1 mM acetaminophen are shown.

The selectivity of the colorimetric glucose sensor was also tested by observing the interference effects from ascorbic acid, uric acid, and acetaminophen. The colorimetric signal, and its hue value at 1 mM glucose barely changed even upon the addition of the interfering species (**Figure 3-8**), exhibiting selectivity towards detection of glucose.

Table 3-1. Glucose concentration analysis of real samples. For the analysis with PANi/ITO/carbon electrode, the average and standard deviation of n=3 (Cola beverage), n=4 (orange juice) are given. For spectroscopic assay, n=4 for both samples.

Sample	PANi/ITO/carbon electrode	Spectroscopic assay
Coca-Cola (g/100 mL)	2.14 ± 0.04	2.16 ± 0.02
Orange juice (g/100 mL)	1.99 ± 0.17	1.96 ± 0.02

Glucose concentration of real food samples were also analyzed with the PANi/ITO/carbon paper electrodes. Commercial beverages (Coca-cola and orange juice) were 500-fold diluted with PBS (pH 5.0) buffer, and the colorimetric signals of PANi were observed 20s after the application of 0 V (vs. printed Ag/AgCl) potential. The colorimetric signals of real samples were then converted to their hue values, and the glucose concentration was calculated according to the calibration curve shown in Figure 5c. The results were compared with those obtained by the commercial spectroscopic assay (**Table 3-1**). By performing a *t*-student test, it can be concluded with a confidence level of 95%, that there are no significant differences between the mean values of glucose concentration obtained from both methods.

3.4. Conclusion

A paper-based electrochemical sensor combined with electrochromic materials enabling rapid, reusable colorimetric sensing was fabricated. Depending on the catalytic materials introduced on the working electrode, the change in the concentration of various analytes could be perceived by the color shift of electrochromic materials at the counter electrode. Colorimetric signals of the deposited electrochromic materials could be clearly observed by the deposition of ITO nanoparticles on screen-printed carbon electrodes, thus allowing detection of analytes without the need for additional readout devices. In this work, the detecting performance of paper-based colorimetric sensor was demonstrated by utilizing polyaniline as the electrochromic indicator. Color change depending on the concentrations of hydrogen peroxide and glucose could be easily perceived with the

naked eye. Glucose concentration of real food samples were also analyzed and compared with the spectroscopic method data to demonstrate the reliability of the paper-based electrochromic sensor. Furthermore, the ITO nanoparticle layer enabled the employment of Prussian Blue, another widely used electrochromic material. In conclusion, we demonstrated a colorimetric sensor concept which utilizes paper substrates as a platform for various electrochromic materials, even without the deposition of conductive metals. This introduces a cost-effective, convenient colorimetric sensor capable of large-scale fabrication. With appropriate power sources, this concept could contribute to the realization of POC devices.

3.5. References

(1) W. Gao, M. Saqib, L. Qi, W. Zhang and G. Xu, *Curr. Opin. Electrochem.*, 2017, **3**, 4–10.

(2) J. Liu, Z. Geng, Z. Fan, J. Liu and H. Chen, *Biosens. Bioelectron.*, 2019, **132**, 17–37.

(3) Z. Yu, Y. Tang, G. Cai, R. Ren and D. Tang, *Anal. Chem.*, 2019, **91**, 1222–1226.

(4) N. Colozza, K. Kehe, G. Dionisi, T. Popp, A. Tsoutsoulopoulos, D. Steinritz, D. Moscone and F. Arduini, *Biosens. Bioelectron.*, 2019, **129**, 15–23.

(5) R. Cánovas, M. Parrilla, P. Blondeau and F. J. Andrade, *Lab Chip*, 2017, **17**, 2500–2507.

(6) E. Noviana, C. P. McCord, K. M. Clark, I. Jang and C. S. Henry, *Lab Chip*, 2020, **20**, 9–34.

(7) S. Chaiyo, E. Mehmeti, W. Siangproh, T. L. Hoang, H. P. Nguyen, O. Chailapakul and K. Kalcher, *Biosens. Bioelectron.*, 2018, **102**, 113–120.

(8) A. W. Martinez, S. T. Phillips, M. J. Butte and G. M. Whitesides, *Angew. Chem. Int. Ed.*, 2007, **46**, 1318–1320.

(9) A. W. Martinez, S. T. Phillips and G. M. Whitesides, *Proc. Natl. Acad. Sci. U. S. A.*, 2008, **105**, 19606–19611.

(10) R. Derda, A. Laromaine, A. Mammoto, S. K. Y. Tang, T. Mammoto, D. E. Ingber and G. M. Whitesides, *Proc. Natl. Acad. Sci. U. S. A.*, 2009, **106**, 18457–18462.

(11) Z. Nie, C. A. Nijhuis, J. Gong, X. Chen, A. Kumachev, A. W. Martinez, M. Narovlyansky and G. M. Whitesides, *Lab Chip*, 2010, **10**, 477–483.

(12) F. Güder, A. Ainla, J. Redston, B. Mosadegh, A. Glavan, T. J. Martin and G. M. Whitesides, *Angew. Chemie - Int. Ed.*, 2016, **55**, 5727–5732.

(13) G. G. Morbioli, T. Mazzu-Nascimento, A. M. Stockton and E. Carrilho, *Anal. Chim. Acta*, 2017, **970**, 1–22.

(14) K. Yamada, H. Shibata, K. Suzuki and D. Citterio, *Lab Chip*, 2017, **17**, 1206–1249.

(15) W. J. Zhu, D. Q. Feng, M. Chen, Z. D. Chen, R. Zhu, H. L. Fang and W. Wang, *Sensors Actuators, B Chem.*, 2014, **190**, 414–418.

(16) E. Rafatmah and B. Hemmateenejad, *Microchim. Acta*, 2019, ***186*** (11).

(17) H. Liu and R. M. Crooks, *Anal. Chem.*, 2012, **84**, 2528–2532.

(18) F. Zhang, T. Cai, L. Ma, L. Zhan and H. Liu, *Sensors (Switzerland)*, 2017, **17**, 1–10.

(19) H. Park, D. S. Kim, S. Y. Hong, C. Kim, J. Y. Yun, S. Y. Oh, S. W. Jin, Y. R. Jeong, G. T. Kim and J. S. Ha, *Nanoscale*, 2017, **9**, 7631–7640.

(20) J. Rho, S. Y. Yeon and T. D. Chung, *Anal. Chem.*, 2020, **92**, 8776–8783.

(21) W. Xu, K. Fu and P. W. Bohn, *ACS Sensors*, 2017, **2**, 1020–1026.

(22) S. Ranjbar, M. Amin, F. Nejad, C. Parolo, S. Shahrokhian and A. Merkoç, *Anal.*

Chem. 2019, **91**, 23, 14960–14966.

(23) X. Zhang, Y. Jing, Q. Zhai, Y. Yu, H. Xing, J. Li and E. Wang, *Anal. Chem.*, 2018, **90**, 11780–11784.

(24) D. D. Liana, B. Raguse, J. J. Gooding and E. Chow, *ACS Appl. Mater. Interfaces*, 2015, **7**, 19201–19209.

(25) Y. Hu, X. Diao, C. Wang, W. Hao and T. Wang, *Vacuum*, 2004, **75**, 183–188.

(26) G. S. Belo, B. J. P. da Silva, E. A. de Vasconcelos, W. M. de Azevedo and E. F. da Silva, *Appl. Surf. Sci.*, 2008, **255**, 755–757.

(27) T. O. L. Sunde, E. Garskaite, B. Otter, H. E. Fossheim, R. Sæterli, R. Holmestad, M.-A. Einarsrud and T. Grande, *J. Mater. Chem.*, 2012, **22**, 15740.

(28) D. D. Liana, B. Raguse, J. J. Gooding and E. Chow, *ACS Appl. Mater. Interfaces*, 2015, **7**, 19201–19209.

(29) M. Aller-Pellitero, S. Santiago-Malagón, J. Ruiz, Y. Alonso, B. Lakard, J.-Y. Hihn, G. Guirado and F. J. del Campo, *Sensors Actuators B Chem.*, 2020, **306**, 127535.

(30) C. Legnani, C. Vilani, V. L. Calil, H. S. Barud, W. G. Quirino, C. A. Achete, S. J. L. Ribeiro and M. Cremona, *Thin Solid Films*, 2008, **517**, 1016–1020.

(31) Y.-T. Cheng, J.-J. Ho, C.-K. Wang, W. Lee, C.-C. Lu, B.-S. Yau, J.-L. Nain, S.-H. Chang, C.-C. Chang and K. L. Wang, *Appl. Surf. Sci.*, 2010, **256**, 7606–7611.

(32) S.-H. Min, D.-S. Park and C. K. Kim, *Mol. Cryst. Liq. Cryst.*, 2014, **601**, 197–204.

(33) M. Hwang, B. Jeong, J. Moon, S.-K. Chun and J. Kim, *Mater. Sci. Eng. B*, 2011, **176**, 1128–1131.

(34) I. Maksimenko and P. J. Wellmann, *Thin Solid Films*, 2011, **520**, 1341–1347.

(35) J. P. Coleman, A. T. Lynch, P. Madhukar and J. H. Wagenknecht, *Sol. Energy*

Mater. Sol. Cells, 1999, **56**, 395–418.

(36) M. Aller-Pellitero, J. Fremeau, R. Villa, G. Guirado, B. Lakard, J. Y. Hihn and F. J. del Campo, *Sensors Actuators, B Chem.*, 2019, **290**, 591–597.

(37) M. Aller-Pellitero, J. Fremeau, R. Villa, G. Guirado, B. Lakard, J. Y. Hihn and F. J. del Campo, *Sensors Actuators, B Chem.*, 2019, **290**, 591–597.

(38) M. A. Pellitero, A. Guimerà, M. Kitsara, R. Villa, C. Rubio, B. Lakard, M.-L. Doche, J.-Y. Hihn and F. Javier del Campo, *Chem. Sci.*, 2017, **8**, 1995–2002.

(39) K. Cantrell, M. M. Erenas, I. de Orbe-Payá and L. F. Capitán-Vallvey, *Anal. Chem.*, 2010, **82**, 531–542.

Chapter 4. Electrochemiluminescence signal enhancement using nanoporous ITO

Parts of this chapter were published as M. Seo[1]; S. Y. Yeon[1]; J. Yun; T. D. Chung*. "Nanoporous ITO implemented bipolar electrode sensor for enhanced electrochemiluminescence" *Electrochim. Acta* **2019**, *314*, 89-95. Parts of figures in this chapter were also used in the thesis of M. Seo.
M. Seo, S. Y. Yeon and T. D. Chung conceived the concept and designed the experiments. S. Y. Yeon. and M. Seo. carried out the experiments. S. Y. Yeon designed the sensor structures and M. Seo optimized nanoporous ITO fabrication protocols.

4.1. Introduction

Bipolar electrode (BPE) is an electrode which induce oxidative and reductive reactions at its two ends by applying electric potential to the electrolyte where the BPE is placed.[1,2] The potential difference between the BPE and the electrolyte solution promotes electrochemical reactions without direct ohmic contact between the BPE and driving electrodes. This wireless character makes BPEs as useful compartments for constructing electrochemical manifolds. It enables facile development of array,[3-5] multiplex systems,[6] or application of other materials.[7] Therefore, the application of BPE has been expanded to various sensors coupled with diverse reporting systems. While a number of previous reporting systems such as colorimetry,[8] fluorescence,[9] and electrochemiluminescence (ECL)[10-12] have been developed, the potential of ECL reporting system is large due to its high sensitivity and low background signal.[13] After the first study from the Manz group which is coupling BPE with the ECL reporting system,[14] theoretical works from the Crooks group expanded the concept to develop actual sensing apparatuses successfully.[15] Therefore, BPE-ECL sensors have been developed to analyze various key analytes involving biologically significant molecules and ions.[16-18]

Meanwhile, Indium tin oxides (ITOs) have been widely used in electrochemical sensor due to high conductivity, optical transmittance, wide electrochemical working voltage window, as well as their feasibility in surface modifying or electrode patterning.[19,20] However, owing to their poor electrocatalytic ability, when they are utilized in electrochemical sensors, ITOs are usually modified with catalytically active metals or enzymes,[21-24] but it leads to additional cost or complicated manufacturing processes.[25]

Nanoporous ITO can be expected to complement the low electrocatalytic activity of ITO materials because it introduces larger surface area and higher density surface defects. Furthermore, additional catalytic capabilities have recently been proposed based on the nanoporous morphology.[26] Although there have been several studies that utilize the nanoporous ITOs as a sensor without surface modification,[27-29] the combination with the BPE system has not yet been realized.

In this report, ITO nanoparticles were deposited on a patterned ITO substrate to implement a nanoporous ITO layer on the cathode of the BPE. BPE is used to detect hydrogen peroxide (H_2O_2) using ECL as a reporting signal. The nanoporous ITO layer significantly lowered the driving voltage and increased the ECL signal intensity, enabling detection with the naked eye even at low driving voltages. In addition, the influence of the nanoporous ITO structure on H_2O_2 detection is investigated by changing the thickness of the nanoporous layer that can be easily adjusted by modifying the spin coating process. I explored the reasons for this ECL enhancement in consideration of the morphology of porous layer and surface area expansion.

4.2. Experimental

4.2.1. Materials

Acetic acid (≥ 99.7%, ACS reagent), potassium chloride (≥ 99.0%, ReagentPlus®), potassium phosphate dibasic, potassium phosphate monobasic, Tris(2,2′-bipyridyl) dichlororuthenium(II) hexahydrate ($Ru(bpy)_3Cl_2 \cdot 6H_2O$, 99.95% trace metals basis), tripropylamine (TPA, ≥99%) were purchased from Sigma Aldrich (St. Louis, Missouri, U.S.A.). Hydrogen peroxide (34.5 %) was purchased from Samchun Chemicals (South Korea). All reagents were used without further purification. All aqueous solutions in this experiment were prepared with ultrapure deionized water (resistivity ~18.2 MΩ) produced by NANO pure Diamond (Barnstead, New Hampshire, U.S.A.). H_2O_2 analyte solutions were prepared with 0.1 M phosphate buffered saline (PBS; pH 6.9) as the electrolyte, and the ECL solution consisted of 5 mM $Ru(bpy)_3^{2+}$ and 25 mM TPA in 0.1 M phosphate buffered saline (PBS; pH 6.9). ITO coated glass was purchased from Techinstro (Yadav Nagar, Nagpur Maharashtra, India). Silver wire (dia. 0.5 mm) and platinum wire (dia. 0.5 mm) were purchased from Sigma Aldrich (St. Louis, Missouri, U.S.A.).

For the chip fabrication and ITO etching process, Hexamethyldisilazane (HMDS) was obtained from J. T. Baker (Phillipsburg, New Jersey, U.S.A.), photoresist (PR; AZ 4620) and developer (AZ 400K) from Merck (Darmstadt, Germany), SU-8 from Microchem (Westborough, MA, U.S.A.), TIN etchant (TE-100) from Transene Company (Danvers, MA, U.S.A.). Poly(dimethylsiloxane) (PDMS) monomer and curing agent from Dow Corning (Midland, MI, U.S.A.), ITO nanoparticle powder (~30 nm diameter) from Lihochem (Taiwan).

External voltage upon the BPE was applied by IviumStat electrochemical

workstation (the Netherlands). Cyclic voltammetry and electrochemical impedance spectroscopy (EIS) in the three electrode system were performed by a CHI 604 potentiostat (CH Instruments, TX, U.S.A.) and Reference 600 (Gamry Instruments, PA, U.S.A.), respectively. The Digital camera (Canon EOS 750D, ISO 6400) and microscope (Nikon TE2000U) were used for optical measurements.

The heating process during nanoporous ITO fabrication was done with a tube furnace [Thermal CVD System, SciEnTech], and the morphology of the fabricated nanoporous ITO films was observed by focused ion beam equipped with a field-emission scanning electron microscope (Helios 650, FEI, U.S.A.).

4.2.2. Fabrication of nanoporous indium tin oxide BPEs

ITO microband electrodes of 22 mm length and 1 mm width were prepared by the following steps. ITO coated glass was subsequently cleaned with ethanol, acetone and deionized water, then dried at 100 ℃ for 5 min. HMDS was spin coated on the ITO coated glass, and baked at 110 ℃ for 1.5 min, followed by PR spin coating and baking at 100 ℃ for 1.5 min. After being covered with a mask bearing the BPE pattern, the ITO glass was illuminated with UV light (365 nm) for 20 s. The PR pattern was developed with AZ 400K developer and baked at 120 ℃ for 15 min. Then, the ITO was etched using TE-100 etchant for 15 min. Finally, remains of PR were eliminated with acetone.

ITO nanoparticles were deposited on the patterned ITO substrate by modifying a previously reported method.[30] First, the patterned ITO substrates were washed by sonication in acetone, isopropanol and water for 20 minutes each, followed by air plasma treatment in order to remove residual impurities. Meanwhile, the ITO

nanoparticles were washed in acetone and ethanol several times, followed by dispersion in 5 M acetic acid/ethanol. To reduce the aggregated ITO nanoparticles, the dispersed ITO nanoparticles were mildly centrifuged, and the resulting supernatant was used as the spin coating solution. Nanoporous ITO layers of varying thicknesses could be obtained by controlling the number of spin coating processes, where the spin coated substrates were placed on a hot plate at 100 ℃ for 10 min between each spin coating process. To ensure the formation of uniform nanoparticle layers, nanoporous ITO layers spin coated more than 2 times were studied in this work. The anodic pole (ECL reporting pole) of the BPE was covered by Kapton tape during the spin coating process, enabling selective deposition of ITO nanoparticles on the cathodic pole (H_2O_2 detecting pole). ITO nanoparticles deposited on regions other than the ITO pattern were carefully removed with Kapton tape and an ethanol swab. Afterwards, the films were annealed in two steps; first at 500℃ in atmospheric air for 1 h, and then at 300℃ in 5% H_2 / Argon gas for 1 h to raise the conductivity of the ITO films.[31,32]

The mold for PDMS channels was prepared by the following steps. Silicon wafer was washed with piranha solution for 20 min and baked at 200 ℃ for 2 min. SU-8 was spin coated on the silicon wafer and baked at 65 ℃ for 2 min and at 95 ℃ for 7 min. The SU-8 layer was illuminated with UV light through a mask with a microchannel pattern for 20 s. Then, the SU-8 pattern was developed with SU-8 remover for 2 min. The patterned wafer was baked at 200℃ for 10 min, and 65℃ for 5 min. For the fabrication of PDMS channels, the wafer was attached on the plate, and PDMS monomer and curing agent (10:1) was filled and baked at 60 ℃ for 2 h. Finally, the PDMS cover was cut to fit the shape of the ITO electrode substrate and attached onto it.

4.2.3. Optical Analysis

The reporting and detecting channels of the nanoporous ITO BPE chip were filled with ECL solution and H_2O_2 solution, respectively. 0.1 M phosphate buffered saline (PBS) (pH 7.0) containing 5 mM $Ru(bpy)_3Cl_2 \cdot 6H_2O$ and 25 mM TPA constituted the ECL solution. H_2O_2 samples of different concentrations (2 M to 5 mM) in 0.1 M PBS (pH 7.0) were independently prepared. For the ECL detection, constant potential (1.9 V) was applied to the two terminals with the aid of a potentiostat via Ag/AgCl wires. Then, the ECL images were obtained in a dark room with a digital camera with an exposure time of 10 s. ECL intensities of the images were analyzed with the ImageJ software.

4.2.4. Electrochemical Methods

Conventional electrochemical characterization of nanoporous ITO electrodes was conducted by a three electrode system with an Ag/AgCl (3 M NaCl) as the reference electrode, and Pt mesh as the counter electrode. The electrical contact with nanoporous ITO electrodes was made by attaching aluminum conductive tape on the ITO substrate, and a portion of the electrode was exposed to the solution using an electroplating tape (3M™ Electroplating Tape 470). Electrochemical impedance spectroscopy (EIS) measurements were done over a frequency range of 10 kHz to 0.05 Hz, with an AC input of 10 mV amplitude superimposed on the DC offset potential.

4.3. Result and discussion

4.3.1. Design of the BPE microchip and the sensing system

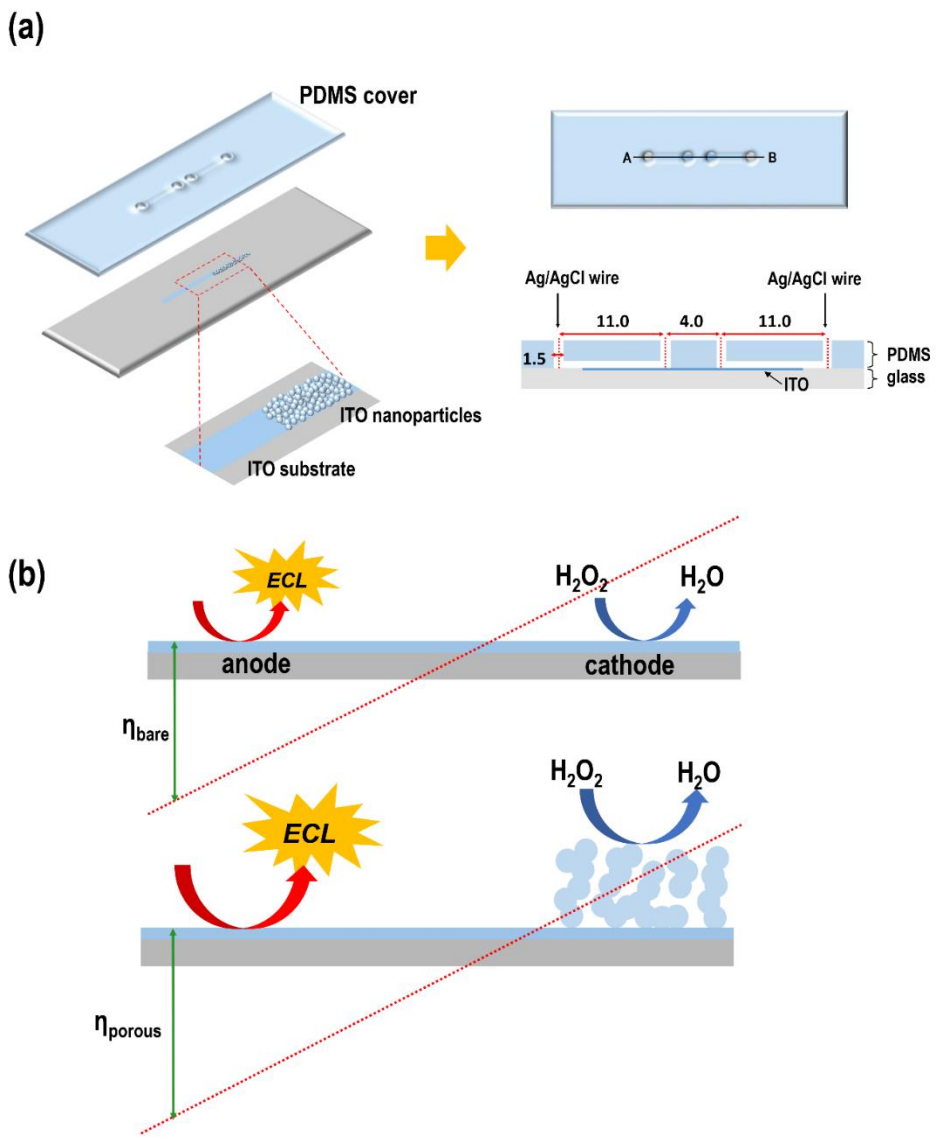

Figure 4-1. (a) Design of the nanoporous BPE microchip. The upper right-hand figure shows the top view of the BPE system, whereas the lower right-hand figure depicts the cross section of the BPE system along line AB. The units of measurements are in mm. (b) Schematic diagram of the H_2O_2 sensing system

involving the BPE. (η: overpotential applied on the anodic poles of BPE) **Figure 4-1** was published in *Electrochim. Acta*, 314, "Nanoporous ITO implemented bipolar electrode sensor for enhanced electrochemiluminescence" M. Seo; S. Y. Yeon; J. Yun, T. D. Chung*, 89-95, Copyright Elsevier (2019).

As shown in **Figure 4-1a**, the BPE microchip was made by following process. The PDMS cover which has 90 μm deep microchannels is fabricated to form the closed channel of the BPE, separating the detecting channel and reporting channel. The nanoporous ITO layer coated cathodic pole operates as the H_2O_2 detecting electrode, whereas the bare ITO anodic pole is the ECL reporting electrode. To make a complete microchip for the BPE sensing system, the transparent PDMS cover was attached on the ITO coated glass. Two driving electrodes, AgCl/Ag wires, were placed in the reservoirs (diameter of 1.5 mm) which was drilled on both ends of the PDMS channel. The detection of H_2O_2, an important indicator of metabolism, was performed to confirm that nanoporous ITO layered BPE microchips can successfully improve electrochemiluminescence (ECL) signals (**Figure 4-1b**). When a total potential (ΔE_{tot}) is applied by the driving electrode, uniform electric field is generated throughout the electrolyte solution. The electrode potential (ΔE_{elec}) is determined according to the ratio of the length of the electrode and the channel. The oxidation of $Ru(bpy)_3^{2+}$ is combined with the reduction of H_2O_2, and ECL reports the concentration of H_2O_2.

4.3.2. Characterization of nanoporous Indium Tin Oxide layer

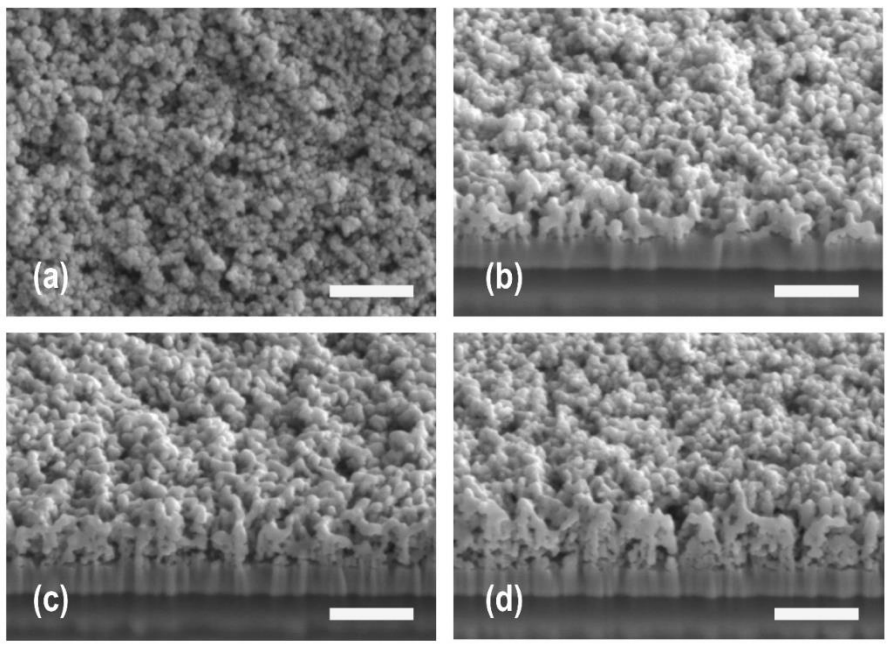

Figure 4-2. (a) Top view Field-Emission Scanning Electron Microscope (FESEM) of nanoporous ITO electrode spin coated 2 times. Cross section FESEM images of electrodes spin coated (b) 2 times, (c) 3 times, and (d) 4 times. The scale bar represents 500 nm. **Figure 4-2** was published in Electrochim. Acta, 314, "Nanoporous ITO implemented bipolar electrode sensor for enhanced electrochemiluminescence" M. Seo; S. Y. Yeon; J. Yun, T. D. Chung*, 89-95, Copyright Elsevier (2019).

In order to characterize the nanoplastic ITO layer formed on the BPE, ITO nanoparticles were deposited on a planar ITO substrate without patterns under the same spin coating conditions. As a result, the structure of the nanoporous ITO electrode was examined by a field emission scanning electron microscope (FESEM)

(**Figure 4-2**). The cross-sectional FESEM image shows the porous structure of an electrode formed by accumulation of ITO nanoparticles. The pore size ranges from tens of nanometers to hundreds of nanometers, and the porous layer thickness was proportional to the number of spin coating processes. Throughout the paper, the nanoporous ITO electrode 'ITO xn' will be represented, where n represents the number of spin coating processes.

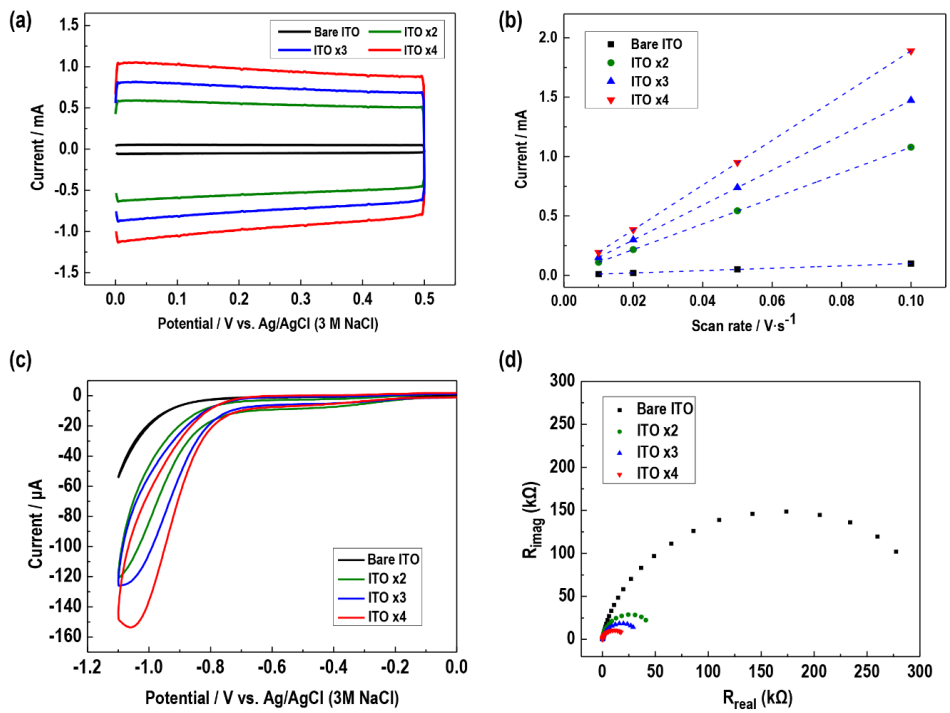

Figure 4-3. (a) The charging current of nanoporous ITO electrodes measured by cyclic voltammetry in 0.1 M phosphate buffered saline solution, scan rate 50 mV/s. (b) The charging current obtained by the average of anodic and cathodic charging currents at 0.250 V (vs. Ag/AgCl (3 M NaCl)) are plotted against various scan rates (10, 20, 50, 100 mV/s). (c) Cyclic Voltammogram of bare ITO, ITO x2, ITO x3 and ITO x4 electrodes in 5 mM H_2O_2, scan rate 50 mV/s. (d) Electrochemical impedance

spectroscopy (EIS) data of bare ITO, ITO x2, ITO x3 and ITO x4 electrodes in 5 mM H_2O_2, where the DC potential is set to - 0.75 V. **Figure 4-3** was published in Electrochim. Acta, 314, "Nanoporous ITO implemented bipolar electrode sensor for enhanced electrochemiluminescence" M. Seo; S. Y. Yeon; J. Yun, T. D. Chung*, 89-95, Copyright Elsevier (2019).

To measure the electrochemical active surface area (ECSA) of the nanoporous ITO electrodes, cyclic voltammetry in 0.1 M phosphate buffered saline solution was performed. The charging current regularly increases as the nanoporous ITO layer increases, ensuring the conductivity of the electrode and accessibility of the nanopores (**Figure 4-3a**). The relative ECSA value can be calculated by fitting the charging current against the scan rate (**Figure 4-3b**). This slope values were utilized to derive the relative ECSA values, which were calculated by dividing the slope values of ITO x2, ITO x3 and ITO x4 electrodes by the slope values of the bare ITO.[33] The slope values and relative ECSA values are in **Table 4-1**.

The electrocatalytic characteristics of nanoporous ITO electrodes for H_2O_2 reduction were measured by cyclic voltammetry and electrochemical impedance spectroscopy (EIS). **Figure 4-3c** shows the cyclic voltammogram of the bare ITO and the nanoporous ITO x2, x3 and x4 electrodes measured in 5 mM H_2O_2. The cathodic current of the nanoporous ITO increased significantly compared to that of the bare ITO electrode, and the onset potential shifted towards positive potential. The EIS measurement data in **Figure 4-3d** show the same trend of significantly decreasing resistance as the porous ITO layer thickens.

Table 4-1. The slope of the plot shown in **Figure 4-3b** and relative ECSA values of Bare ITO electrode, ITO x2, ITO x3 and ITO x4 electrodes.

Electrode	Slope	Relative ECSA
Bare ITO	9.91×10^{-7}	1.00
ITO x2	1.08×10^{-5}	10.9
ITO x3	1.47×10^{-5}	14.8
ITO x4	1.88×10^{-5}	19.0

4.3.3. Optical analysis of H_2O_2 detection

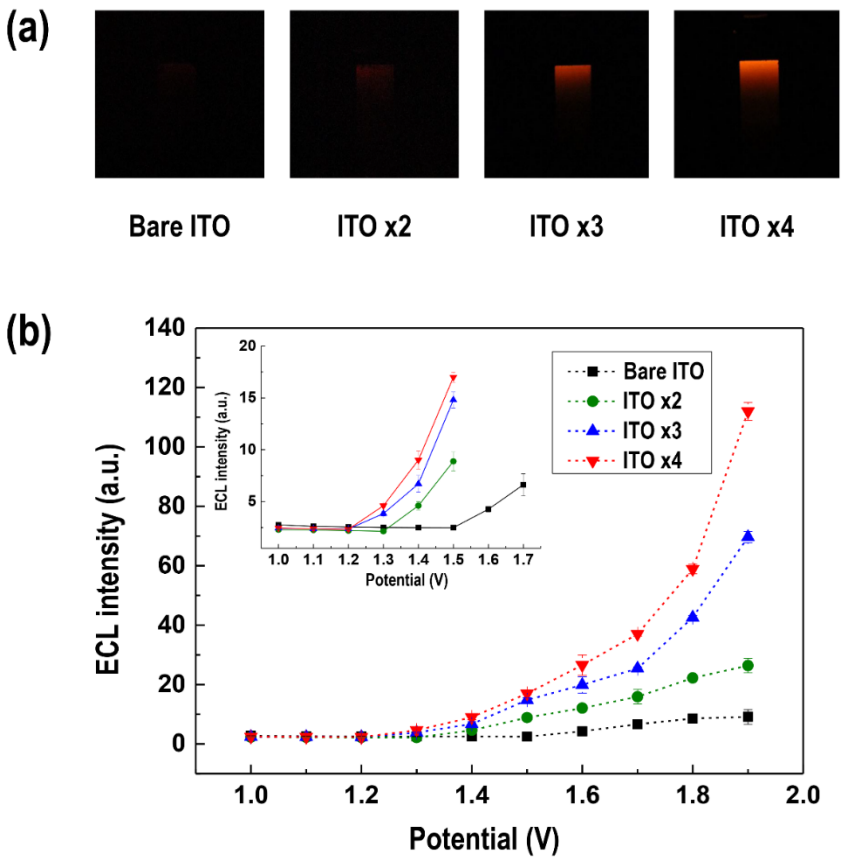

Figure 4-4. H_2O_2 sensing system with four BPEs with different depths of ITO

nanoporous layers. (a) ECL images obtained from a 5 mM H_2O_2 solution under constant voltage of 1.9 V (b) ECL intensities of BPEs from 5 mM H_2O_2 depending on the applied voltage, where the inset shows the enlarged view of ECL intensities at mild potentials. **Figure 4-4** was published in Electrochim. Acta, 314, "Nanoporous ITO implemented bipolar electrode sensor for enhanced electrochemiluminescence" M. Seo; S. Y. Yeon; J. Yun, T. D. Chung*, 89-95, Copyright Elsevier (2019).

Since H_2O_2 is involved in various biological events such as cellular function and signaling processes, it is practically important to develop reliable, sensitive, and low-cost methods for H_2O_2 detection.[34] As described in the previous section, detection of H_2O_2 with BPE was performed to verify the ECL signal amplification effect due to nanoporous ITO electrode. In the H_2O_2 analysis, three types of BPE microchips (ITO x2, ITO x3, and ITO x4) with different porous layer thicknesses and bare ITO BPE were used. In **Figure 4-4a**, ECL images of 5 mM H_2O_2 are shown, where stronger ECL signals can be clearly observed according to the deposition of the nanoporous ITO layer. This means that the nanoporous ITO introduced BPE can operate at an external voltage lighter than that required for BPE with bare ITO. This function is further illustrated in **Figures 4-4b**, in which ECL signals of various BPEs toward 5mM H_2O_2 are measured according to the driving voltage. As shown in the inset of **Figure 4-4b**, a clear decrease of the onset potential was observed in BPE with a thicker layer of nanoporous ITO. In order to obtain sufficient sensitivity to analyte detection, 1.9V was selected as the driving voltage in the following experiment.

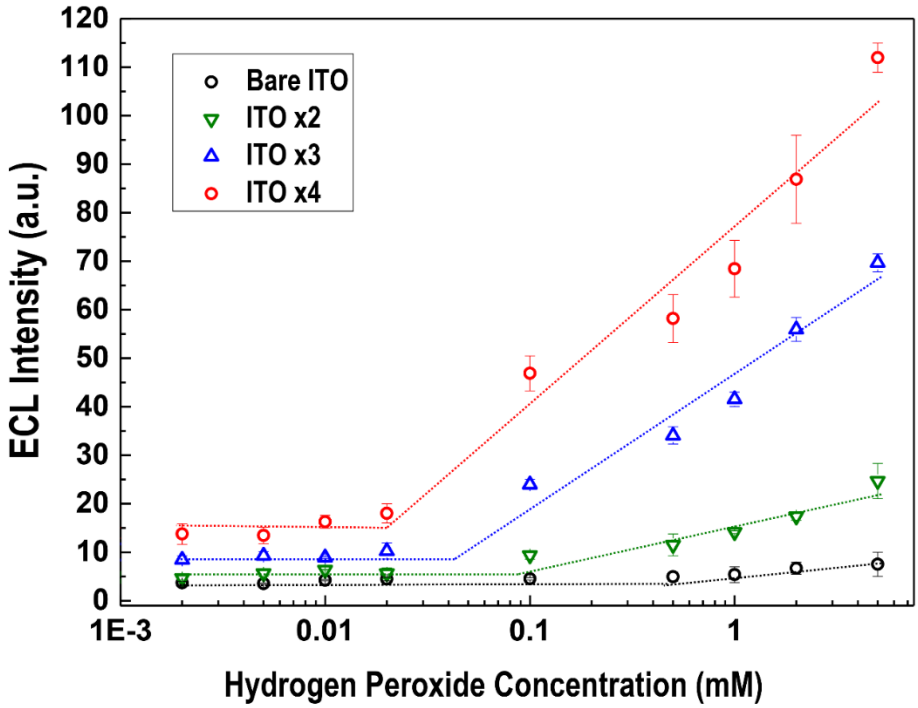

Figure 4-5. ECL intensities depending on the analyte (H_2O_2) concentration. The dotted lines are added to guide the linear range. **Figure 4-5** was published in Electrochim. Acta, 314, "Nanoporous ITO implemented bipolar electrode sensor for enhanced electrochemiluminescence" M. Seo; S. Y. Yeon; J. Yun, T. D. Chung*, 89-95, Copyright Elsevier (2019).

The H_2O_2 detection capacity of BPE was observed by measuring the ECL signals with concentration from 2 μM to 5 mM (**Figure 4-5**). A good linear relationship was found between the logarithm of the H_2O_2 concentration and the ECL intensity. The signal intensity and slope of the calibration curve increased as the nanoporous ITO layer increased, indicating that the H_2O_2 reduction activity of the nanoporous ITO electrode was improved. The linear range and detection limit (LOD) obtained from the calibration curve in **Figure 4-5** are summarized in **Table 4-2**, where LOD was

calculated as the lowest H_2O_2 concentration with the signal three standard deviations above the blank solution. The LOD value greatly decreases as the nanoporous layer increases, and for ITO x4 electrodes, the lowest LOD value 21.86 μM is acquired. The degree of change in LOD according to the increase in the nanoporous layer shows that the effect of the nanoporous structure on the signal intensity and the sensitivity of BPE.

Table 4-2. The linear range and LOD of nanoporous BPEs.

Electrode	Linear range (mM)	LOD (μM)
Bare ITO	0.5 – 5	271.97
ITO x2	0.1 – 5	70.42
ITO x3	0.1 – 5	43.98
ITO x4	0.02 – 5	21.86

One of the reasons for improving ECL intensity in nanoporous ITO introduced BPE may be that the surface area of the cathode has increased. Previous studies have reported advantageous ECL intensity when tuning relative regions of the anode and cathode.[15,35,36] As shown in **Figure 4-1b**, the enlarged area of the cathode (nanoporous ITO) compared to the anode (bare ITO) made increased anodic overpotential, leading to enhanced ECL with a thicker layer of nanoporous ITO even under the same driving voltages.

4.3.4. Nanoconfinement effects of nanoporous structures towards H_2O_2 detection

I also explored the principles for enhancing the ECL of nanoporous ITO BPE in

terms of their structural properties and their electrocatalytic effects on H_2O_2 reduction. Nanoporous electrodes can increase the catalytic effect by trapping reactant molecules in nanopores to increase the interaction between the reactant and the electrode surface. This catalytic mechanism based on the nanoporous structure has been proposed in previous reports, called as the 'nanoconfinement effect'.[26,37]

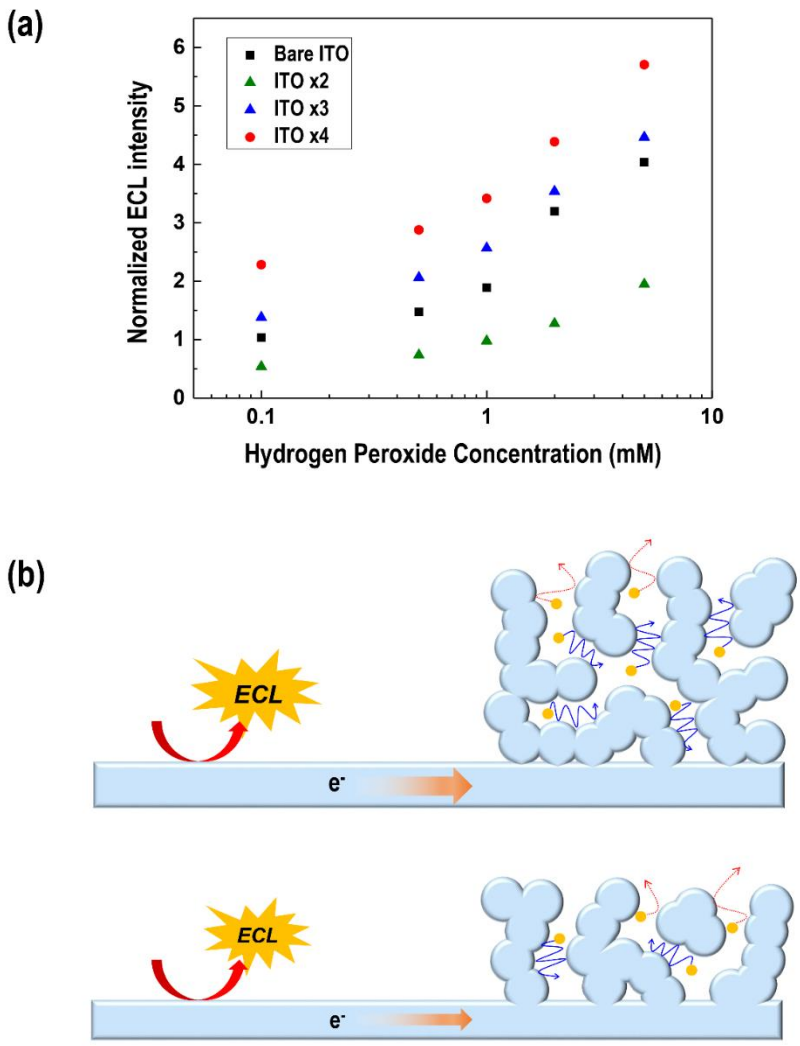

Figure 4-6. (a) ECL intensities of bareITO, ITO x2, x3, and x4 implemented BPEs, normalized by the relative ECSA values through the following equation; Normalized

ECL intensity = {(Measured ECL intensity) – (Background ECL intensity)} / (ECSA value). The background ECL intensity which is the light intensity when no voltage is applied to the BPE, is subtracted to eliminate the background noise. (b) Scheme of reactants in the nanoconfined space of nanoporous ITO layers with differing thickness. The orange circles represent the reactant molecules, and the arrows represent the simplified trajectories of the reactants. The blue, solid arrows demonstrate increased interaction between the reactant molecules and the electrode due to nanoconfinement effects. The red dashed arrows depict reactants in the shallow regions of the nanoporous structure, which are less likely to be confined in the nanopores. **Figure 4-6** was published in Electrochim. Acta, 314, "Nanoporous ITO implemented bipolar electrode sensor for enhanced electrochemiluminescence" M. Seo; S. Y. Yeon; J. Yun, T. D. Chung*, 89-95, Copyright Elsevier (2019).

Comparing the reduction activity of H_2O_2 activity of nanoporous ITO BPE with different layer thicknesses, it is possible to investigate the nanoconfinement effect resulting from nanoporous morphology. Since the degree of H_2O_2 reduction activity generated in the nanoporous ITO layer is reflected in the ECL signal intensity, the catalytic effect is can be determined without direct measurement of the current through the BPE. To exclude increases originating from the surface area of nanoporous ITO and to evaluate and compare ECL signal intensity, the ECL intensities of nanoporous ITO (formerly shown in **Figure 4-5**) were normalized by relative ECSA value (listed in **Table 4-1**).[26] The normalized ECL values of the nanoporous ITO BPE of x2, x3, and x4 layers for various H_2O_2 concentrations are shown in **Figure 4-6a**. ITO x3 and ITO x4 BPE have higher ECL intensity than bare ITO BPE, and the ECL signal is strengthened as the thickness of the nanoporous ITO

layer increases.

As the surface area is normalized, the difference in catalyst factors of the ITO x2, x3, and x4 electrodes insists the extent of the 'nanoconfined space'. Therefore, this suggests that the improvement of normalized ECL signals with the increase of the nanoporous ITO layer contributes to the improvement of H_2O_2 reduction activity due to the limited space of ITO nanopores. As shown in the **Figure 4-6b**, The thicker nanoporous layers lead to larger proportion of deep nanopores (i.e. extended nanoconfined space), and it intensify degrees of reactant confinement and catalyze the faradaic reactions.

Therefore, I analyzed the ECL signal enhancement of nanorpous ITO compared to the signal from the bare ITO anode to investigate the effect of the nanoconfinement effects of nanoporous implemented ITO. This is the first time that the nanoconfinement effects has been verified in a system that does not directly measure the faradaic current of nanoporous electrode.

4.4. Conclusion

I developed a new nanoporous ITO BPE-based detection system that transforms the cathode into a nanoporous ITO layer, leading to LOD improvement and higher sensitivity to H_2O_2 detection. By increasing the thickness of the layer of nanoporous ITO, detection can be further improved. Other surface modifications of ITO such as metal nanoparticles or enzyme adhesion were not made, bypassing the cost problem or concerns of electrode failure due to surface contamination. The enhanced efficiency of the sensing capability allowed the BPE to detect H_2O_2 under a relatively low potential of 1.9 V. In the process of further investigating the enhanced sensing

capabilities of nanoporous ITO BPE, the presence of nanoporous electrodes was indirectly demonstrated with the contribution of the BPE-ECL system.

Since ECL is a widely used detection system throughout BPE-based electrochemical sensing, the development of greatly sensitive nanoporous electrodes implemented sensing devices can realize direct detection with the naked eye. With these advantages, this system has proven to be a candidate for further expansion to portable and on-site sensing devices.

4.5. References

(1) S.E. Fosdick, K.N. Knust, K. Scida, R.M. Crooks, *Angew. Chem. Int. Ed.* 2013, **52**, 10438–10456.

(2) G. Loget, D. Zigah, L. Bouffier, N. Sojic, A. Kuhn, *Acc. Chem. Res.* 2013, **46**, 2513–2523.

(3) K.-F. Chow, F. Mavré, J.A. Crooks, B.-Y. Chang, R.M. Crooks, A Large-Scale, Wireless Electrochemical Bipolar Electrode Microarray, *J. Am. Chem. Soc.* 2009, **131**, 8364–8365.

(4) S. Hu, J. Gao, *ACS Appl. Mater. Interfaces.* 2019, **11**, 1117–1124.

(5) V. Eßmann, C. Santana Santos, T. Tarnev, M. Bertotti, W. Schuhmann, *Anal. Chem.* 2018, **90**, 6267–6274.

(6) M.-S. Wu, Z. Liu, H.-W. Shi, H.-Y. Chen, J.-J. Xu, *Anal. Chem.* 2015, **87**, 530–537.

(7) X. Lin, L. Zheng, G. Gao, Y. Chi, G. Chen, *Anal. Chem.* 2012, **84**, 7700–7707.

(8) W. Xu, K. Fu, P.W. Bohn, *ACS Sens.* 2017, **2**, 1020–1026.

(9) J.P. Guerrette, S.J. Percival, B. Zhang, *J. Am. Chem. Soc.* 2013, **135**, 855–861.

(10) X. Zhang, S.-N. Ding, *Biosens. Bioelectron.* 2017, **94**, 47–55.

(11) M. Sentic, M. Milutinovic, F. Kanoufi, D. Manojlovic, S. Arbault, N. Sojic, *Chem. Sci.* 2014, **5**, 2568–2572.

(12) M. Sentic, S. Arbault, B. Goudeau, D. Manojlovic, A. Kuhn, L. Bouffier, N. Sojic, *Chem. Commun.* 2014, **50**, 10202–10205.

(13) Q.-M. Feng, J.-B. Pan, H.-R. Zhang, J.-J. Xu, H.-Y. Chen, 2014, **50**, 10949–10951.

(14) A. Arora, J.C.T. Eijkel, W.E. Morf, A. Manz, *Anal. Chem.* 2001, **73**, 3282–3288.

(15) W. Zhan, J. Alvarez, R.M. Crooks, *J. Am. Chem. Soc.* 2002, **124**, 13265–13270.

(16) K.-F. Chow, F. Mavré, R.M. Crooks, *J. Am. Chem. Soc.* 2008, **130**, 7544–7545.

(17) M.-S. Wu, D.-J. Yuan, J.-J. Xu, H.-Y. Chen, *Chem. Sci.* 2013, **4**, 1182–1188.

(18) V. Eßmann, D. Jambrec, A. Kuhn, W. Schuhmann, *Electrochem. Commun.* 2015, **50**, 77–80.

(19) A. El Kasmi, M.C. Leopold, R. Galligan, R.T. Robertson, S.S. Saavedra, K. El Kacemi, E.F. Bowden, *Electrochem. Commun.* 2002, **4**, 177–181.

(20) E. Moore, D. O'Connell, P. Galvin, *Thin Solid Films.* 2006, **515**, 2612–2617.

(21) J. Lin, W. Qu, S. Zhang, Anal. Biochem. 2007, **360**, 288–293.

(22) H. Tian, M. Jia, M. Zhang, J. Hu, *Electrochim. Acta.* 2013, **96**, 285–290.

(23) J.I.A. Rashid, N.A. Yusof, J. Abdullah, U. Hashim, R. Hajian, *Mater. Sci. Eng. C*, 2014, **45**, 270–276.

(24) B. Reuillard, K.H. Ly, P. Hildebrandt, L.J.C. Jeuken, J.N. Butt, E. Reisner, *J. Am. Chem. Soc.* 2017, **139**, 3324–3327.

(25) D.-W. Hwang, S. Lee, M. Seo, T.D. Chung, Anal. Chim. Acta. 2018, **1033**, 1–34.

(26) M. Seo, J.H. Bae, D.W. Hwang, B. Kwak, J. Yun, S.Y. Lim, T.D. Chung,

Electrochim. Acta, 2017, **258**, 90–97.

(27) M.-Y. Wei, R. Huang, L.-H. Guo, J. Electroanal. Chem. 2012, **664**, 156–160.

(28) M. Mierzwa, E. Lamouroux, I. Vakulko, P. Durand, M. Etienne, *Electrochim. Acta,* 2016, **202**, 55–65.

(29) M.A. Aziz, W. Mahfoz, M. Nasiruzzaman Shaikh, M.H. Zahir, A.-R. Al-Betar, M. Oyama, D. Theleritis, Z.H. Yamani, *Electroanalysis,* 2017, **29**, 1683–1690.

(30) P.G. Hoertz, Z. Chen, C.A. Kent, T.J. Meyer, *Inorg.* 2010, **49**, 8179–8181.

(31) O.N. Mryasov, A.J. Freeman, *Phys. Rev. B.* 2001, **64**, 233111.

(32) T. von Graberg, P. Hartmann, A. Rein, S. Gross, B. Seelandt, C. Röger, R. Zieba, A. Traut, M. Wark, J. Janek, B.M. Smarsly, *Sci. Technol. Adv. Mater.* 2011, **12**, 025005.

(33) C.C.L. McCrory, S. Jung, J.C. Peters, T.F. Jaramillo, *J. Am. Chem. Soc.* 2013, **135**, 16977–16987.

(34) T. Wang, H. Zhu, J. Zhuo, Z. Zhu, P. Papakonstantinou, G. Lubarsky, J. Lin, M. Li, *Anal. Chem.* 2013, **85**, 10289–10295.

(35) F. Mavré, K.-F. Chow, E. Sheridan, B.-Y. Chang, J.A. Crooks, R.M. Crooks, *Anal. Chem.* 2009, **81**, 6218–6225.

(36) S.M. Oja, B. Zhang, *ChemElectroChem.* 2016, **3**, 457–464.

(37) J.-H. Han, E. Lee, S. Park, R. Chang, T.D. Chung, *J. Phys. Chem. C.* 2010, **114**, 9546–9553.

국문초록

전기화학센서는 민감도, 신속성, 저비용, 현장 측정 적합성 등의 장점 때문에 다양한 산업에 광범위하게 적용되고 있다. 대사물, 핵산, 단백질, 이온 등 다양한 유형의 분석물질이 분석되어왔다. 첫째, 대표적인 전기화학 센서인 전류센서는 일정한 전위 하에서 전극에서 반응물이 산화되거나 환원될 때 나타나는 전류의 크기가 농도에 비례한다는 사실을 이용하여 분석물질 농도를 측정한다. 예를 들어, 과산화수소는 포도당과 젖산과 같은 대사물의 효소 반응으로부터 생성되며, 바이오센서 및 면역센서에 일반적으로 사용된다. 둘째, 또 다른 대표적인 전기화학센서인 전압센서는 이온선택성을 갖는 막에서 발생하는 전압신호로 이온농도를 분석하는 데 주로 사용된다. 이온농도와 발생 전압은 네른스티안 기울기(59mV/decade)를 따른다. 최근에는 고체 접촉 이온선택성 전극과 소형화 이온 선택성 전극이 광범위한 관심을 받고 있다. 이외에도 전기화학 센서에는 전기화학적 임피던스 센서 및 전도성 센서와 같은 분석 방법도 있다.

Point of care(POC)에 대한 개념이 1980년대 초에 처음 도입된 이후, POC에 대한 많은 연구가 수행되었다. 이는 시간과 장소에 상관없이 사람들이 자신의 건강 상태를 빠르게 확인할 수 있도록 하는 것이다. 이 개념을 구현하기 위해서는 휴대성이 뛰어난 센서의 개발이 필수적이다. 또한 사용이 편리해야 하며 신속하게 결과를 얻을 수 있어야 한다. 이에 최근 전기화학 센서 분야에서는 검출 시간이 짧은 휴대용 센서를

개발하는 연구가 많이 보고되고 있다. 휴대용 센서의 재료를 개발하거나, 자체 동력 시스템 개발 및 신호 전송 시스템에 대한 연구가 이루어져왔다.

먼저 종이, 고분자, 섬유 등 휴대용 소재를 이용한 전기화학 센서가 개발되었다. 종이는 가볍고 친환경적이며, 저비용 센서 플랫폼을 위한 재료로 널리 개발되어 왔다. 환경 및 질병의 현장 진단과 관련하여 기존의 전기화학 센서의 대안으로 종이 기반 전극 개발에 대한 연구가 보고되었다. 마이크로 유체 분석 장치(μPAD) 와 같은 적은 양의 샘플로 분석할 수 있는 연구가 보고되었다. 고분자도 웨어러블 기기와의 접목 가능성이 제기돼 관심을 받고 있다. 폴리이미드, 폴리카보네이트, 및 폴리디메틸실록세인 등이 센서의 구조체로 활용되었다. 종이와 고분자 외에도 섬유와 직물과 같은 소재 또한 휴대용 장치를 만드는 데 사용되어 왔으며, 문신, 렌즈, 패치 등의 웨어러블 센서가 보고되었다. 그러나 이러한 시스템에서는 더 가벼운 물질로 소재를 바꾸기는 했지만 대부분 여전히 외부 전원이나 검출기를 연결해서 사용해오고 있다.

둘째, 자체 동력 시스템인 압전 나노 발전기술은 2006년에 처음 제안된 동작 에너지를 전기로 변환하는 기술이다. 산화아연 나노 와이어는 외부 자극에 반응하고 전압을 발생시키기 위해 사용되었다. 또한 서로 다른 두 물질 사이의 기계적 압축으로 전기를 발생시키는 TENG(Triboelectric Nan Generator)이 개발되었다. 최근에는 몸의 움직임을 인식하고 VR 제어가 가능하다는 것이 보고되었다. 한편, 바이오 연료 셀 시스템을 이용하여 생물학적 유체로부터의 에너지 생산

시스템이 연구되고 있다. 웨어러블 땀 센서가 배터리 없이 BFC에 의해 구동되는 시스템으로 소개되었다.

최근에는 센서의 신호를 분석하는 검출기를 센서에서 분리해 휴대성을 높이는 무선 전송에 대한 연구도 진행되고 있다. 이 시스템은 건강 상태를 지속적으로 모니터링해야 하는 질병으로 고통받는 환자에게 특히 유용하다. 5세대 무선 전송과 같은 이동 통신 기술이 POC에 활용되었다. 땀 속 전해질 수준의 농도를 감지하기 위한 소형화 및 저비용 장치를 개발하기 위해 근거리 통신이 사용되었다. 게다가 자체 전력 시스템의 적용을 확대하기 위해 무선 전송 기술을 TENG에 적용했다. TENG에서 생성된 펄스 전압은 무선으로 수신기로 전송되었다.

요약하자면, POC에 적합한 휴대용 센서 개발을 위해 소재나 방식 측면에서 다양한 연구가 진행되어 왔다. 그러나 이러한 연구들은 실제 활용 단계에 도달하려면 아직 개선할 부분이 많이 남아있다. 휴대용 재료를 활용하는 연구는 여전히 기존의 외부 전원이나 검출기를 사용하기 때문에 휴대성이 부족하다. TENG, BFC와 같은 자체 동력 시스템은 바이오 유체, 모션을 활용하여 작동 환경에서 전력을 생산할 수 있다. 다만 바이오 유체의 경우 안정적인 전력생산이 어려워 추가적인 에너지 저장장치를 사용하고 있으며, TENG의 경우 대부분 동작 감지 시스템에만 제한적으로 활용되어왔다. 무선 전송은 인덕터 간 유도자기장의 원리를 활용하여 전송 거리 범위가 제한되고 사용된 안테나의 크기와 형태에 따라 신호에 영향을 받는다.

따라서 이러한 POC 연구에서 주로 사용되던 전략과 달리, 본

학위논문의 연구들은 전력원과 신호 판독 시스템의 소형화에 초점을 맞추어 POC에 적용하고자 하였다. 또한 휴대용 센서에 알맞게 별도의 신호 처리 없이 육안으로도 ECL과 같은 발광신호를 구별할 수 있도록 신호 세기를 증진시킨 연구도 소개한다.

오늘날 전기화학 센서는 실험실 규모로만 개발되기 보다는 실제 현장에서 활용될 수 있는 수준으로 개발되어야 한다. 의료, 환경, 제약, 식품 등 여러 산업분야에서 POC를 위한 다양한 분석 물질에 대해 간단하고 빠른 센서에 대한 필요성이 높아지고 있다. 앞에서 소개한 것처럼 현재까지 다양한 POC 센서 연구가 이루어져 오고 있고, 향후 자체 동력시스템과 신호 무선전송 등의 여러 기술과 결합되면 POC에 적합한 센서가 멀지 않은 미래에 개발될 것으로 전망된다.

Acknowledgement (감사의 글)

돌이켜보면 연구실에서 보낸 6년이라는 시간이 참 빠르게 지나갔다는 생각과, 웃고 떠들던 찰나들이 머릿속을 스쳐 지나며 슬픈 감정이 앞서는 걸 보니 저는 감사하게도 좋은 사람들을 만나 아름다운 순간들을 참 많이도 남겼나 봅니다. 학위논문을 갈무리 짓는 마지막 글을 작성하는 것을 여태껏 부러 뒤로 미뤄왔는데 늦은 밤 떠오르는 몇몇 얼굴들에 차오르는 이 감정을 글로 남겨보고자 책상 앞에 앉아봅니다.

먼저 지도교수님이신 정택동 교수님께 감사드립니다. 처음 학위과정을 시작했을 때 철없던 저를 교수님께서는 마냥 웃으면서 의견을 나눌 수 있도록 학생의 눈높이에 맞춰서 대해 주셨습니다. 새로운 아이디어가 생각나면 부푼 가슴을 안고 교수님을 찾아 뵈러 달려갔던 그 순간들이 지금까지도 참 좋은 기억으로 남아있습니다. 교수님께서는 제가 연구자로 성장하는 과정에서 누구보다도 인정받고 싶었던 스승이셨습니다. 그래서 제가 한 때 스스로를 닥달하다 자신감을 잃었을 때는 교수님께 그런 약한 제 모습을 들키고 싶지 않아 홀로 길을 잃고 캄캄한 어둠 속에서 헤매기도 했습니다. 교수님께서 그런 저를 알아보시고 주셨던 진심 어린 조언들 마음 깊이 새기고, 앞으로 굳세게 나아가도록 하겠습니다. 다시 한번 감사드립니다.

바쁘신 와중에 기꺼이 시간을 내어 학위논문 심사에 참여해주시고, 연구자로서 가져야할 자세에 대해서 좋은 말씀을 나누어 주셨던 김종원 교수님, 이연 교수님, 황윤정 교수님, 권승용 교수님께 감사드립니다. 연구 내외적으로 제가 생각해 볼만한 것들에 대해 여러 조언을 해 주셔서 졸업을 준비하는 동안 많은 도움이 되었습니다.

함께 동고동락했던 소중한 동료들에게 고마움을 전하고 싶습니다. 늘 융기원의 같은 자리에서 항상 미소로 저를 맞이해 주시고, 학위과정 내내 힘이 되어 주신 융기원 학생들의 정신적 지주 충무 오빠, 마주칠 때마다 웃으면서 인사해주시고 함께 대화할 때마다 조곤조곤 편안하게 말씀해 주셔서 마음이 안정되곤 하는, 어느새 참 정들어버린 은중 언니, 항상 본인보다 타인을 먼저 챙기고 열정을 바쳐 밤새 실험하던 모습이 아직도 생생하고, 연구실 생활을 막 시작한 내게 가족 같은 따뜻한 정을 느끼게 해주었던 모두가 좋아하는 내 첫 공동연구자 정세 오빠, 겉으로는 무뚝뚝하셨지만 늘 후배들에게 먼저 도움을 주려고 하셨고 아마도 커피도 가장 많이 쏘셨던 통 크고 너그러운 우혁 오빠 (평생 컴퓨터 고장 날 때마다 오빠가 생각날 것 같습니다:) 진숙 언니, 우진이와 행복하세요!), 연구실 공동생활에서 학생들이 놓치기 쉬운 부분을 잘 캐치해서 종종 환기해 주셨고, 누구보다도 실험에 진심이셨던 모습이 인상적이었던

부지런한 재호 오빠, 함께 일하는 동안 연구 잘하는 법을 몸소 보여준 멋진 선배이자 항상 나에게 관심과 애정을 주어서 기쁜 일이든 슬픈 일이든 내 이야기를 모두 전하고 싶고 지금도 제일 먼저 편하게 연락할 수 있는 지헌 언니, 다방면에 박학 다식해서 대화하기가 즐거웠고, 정적인 모습에서 동적인 모습으로 변화하는 모습을 보여주어 참 재미있었던 지금은 한층 더 멋있어진 재경 오빠, 공동연구를 가장 많이 했는데 꼼꼼한 성격으로 연구하는 동안 참 많이 의지할 수 있었고, 능력자임에도 불구하고 더욱 성장하기 위해 끊임없이 노력하는 모습이 정말 대단한 겸손왕 민지 언니, 언니가 가장 많은 일을 맡고 있었던 힘들었을 시기에 옆에서 보조하는 역할로 함께 했었는데 멋모르는 어린 후배인 나를 참 많이 배려해주었고 다른 소속의 사람들과 함께 일하는 법을 가르쳐준 프로페셔널한 지혜 언니, 늘 한결같이 성실하고 자기관리 철저한 모습이 멋있었고 격의 없이 대할 수 있게 해주어 솔직한 내 생각을 편하게 이야기 할 수 있어 좋았던, 연구실 생활에 즐거움을 채워준 석희 오빠, 힘들고 어려운 일들도 편안한 표정으로 아무렇지 않게 해내고, 자신이 원하는 인생의 색을 명확히 판단해서 소신 있게 살아가는 모습이 멋있어서 닮고 싶었던 얼리어답터 다혜 언니, 함께했던 시간이 너무 짧아 아쉬웠지만 짧은 시간 동안에도 실험하는 방법을 제대로 전수해 주셨고 늦게까지 실험할 때도 늘 밝고 힘찬 모습이었던 에너제틱 내 사수님 설 언니, 언니가 만든 피피티와 작성한 글을 볼 때마다 이건 노력으로 절대 따라할 수 없다는 생각이 절로 들게 만들었던, 지금도 소속된 팀에서 무조건 활약하고 있을 것 같은 재능러 주희 언니, 자기 일도 잘 해내면서 다른 학생들을 연구 내외적으로 두루두루 잘 챙겼던 따뜻한 선배였고 나를 항상 재미있다고 말 해주는 게 너무 재미있었던 의리 있고 정의로운 다예 언니, 연구실에 들어와 처음 가까워진 사람이 너무 좋은 사람이었어서 내가 연구실에 오게 된 큰 계기 중 하나였고, 나와 희로애락을 함께 나누었던, 항상 모든 일에 꼼꼼하고 준비된 자세로 임해서 의지가 되었던 믿음직한 민아, 늘 밝은 에너지로 주변 사람들을 즐겁게 해주고, 연구도 잘해내는 모습이 한결같았던 내 하나뿐인 멋진 동기이자 진심어린 이야기도 종종 해줬던 인생 2회차 같은 상미 언니, 내공이 많으셔서 우리 연구실에 오신지 얼마 안되었을 때부터 많은 역할을 해 주셨고 동생들에게 도움도 조언도 잘 해주시는 따뜻한 희정 오빠, 코로나 전에 오빠가 항상 외쳐주었던 '밥 고'가 벌써 그립고, 오빠가 종종 열어주는 하늘관찰시간과 같이 달과 별을 찍던 순간들이 오래 기억에 남을 것 같은, 사람을 참 편안하게 해주는 대웅 오빠, 어려운 일이 있을 때마다 앞장서서 봉사하던 모습이 인상적이었고 동생들과 대화할 때도 늘 상대를 존중해주는 느낌을 받게 해주었던, 그리운 에너지팀에서 오랜 시간 함께해 온 정든 지태 언니, 시작부터 지금까지 늘 한결같이 융기원의 중심을 잡아주고 있고, 언니가 없었다면

힘들었던 시기를 어떻게 버텼을까 싶을 정도로 내게 큰 힘이 되어주었던, 이제는 너무 소중한 사람이 된 선미 언니, 대화할 때마다 사람들에게 시원하게 공감을 잘 해주고, 아무도 없는 늦은 밤에도 실험하는 모습을 보니 정말 담력이 센 것 같은, 늘 건강하길 바라는 승희 언니, 남을 배려하고 주변을 잘 챙겨서 동갑이지만 가끔은 언니 같고, 시크한 겉모습 속에 따뜻하고 여린 마음을 가진, 돌이켜보면 많은 우연이 이어져 이제는 인연이 된 것 같은 내 십년지기 원경이, 언제 어디서나 의견을 당당하게 꺼내는게 멋있고 뚝심있게 연구하는 모습이 대단한, 호탕하고 기분 좋은 웃음소리를 가진 창헌 오빠, 어려운 주제를 맡아 힘들게 연구를 해오고 있는데 꼭 좋은 결실을 맺었으면 좋겠고, 오랜 시간 함께하면서 내게 알게 모르게 힘이 되어준 늘 응원하게 되는 동기 재열이, 초반에 함께 연구하다가 다른 팀에서 연구주제를 진행하게 되었는데 이후에도 많은 도움을 주어서 고맙고, 항상 밝은 얼굴로 인사해주어 만날 때마다 기분이 좋아지는 인간 비타민 로사, 배시시 수줍게 웃는 얼굴이 자꾸만 놀리고 싶게 만들지만 일할 때는 초집중 모드로 완벽한 일처리를 보여주어 인상적이고 믿음직했던, 늘 도전하는 모습이 멋진 문주, 항상 모두를 진심으로 대하고 세심하게 타인을 챙기는 따뜻한 마음을 가진, 참 좋은 동생이 옆에 있어 행복하다고 느끼게 해준, 오래오래 곁에 두고 싶은 센스쟁이 지용이, 학부생 때부터 봐와서 그런지 내게는 아직도 귀여운 동생인데 후배들을 잘 이끌고 하나라도 더 가르쳐주려는 모습이 멋있고, 지금은 어느새 연구실의 중심이 된 것 같은 아싸인 척 하는 핵인싸 승일이, 붙임성 있고 싹싹하게 사람들에게 먼저 다가가 챙겨주고 이야기를 재미있게 푸는 능력을 가져서 같이 얘기하다 보면 마냥 즐거운, 함께 일을 했을 때도 좋았던 기억 뿐이고 늘 행복하길 바라는 승환이, 힘든 실험과정을 진행해야 하는 주제를 맡아서 고생하는 걸 봐오다 보니 안쓰럽지만 그래도 꿋꿋이 해내는게 대단하고, 속에 많은 흥을 감추고 있는 것 같아 계속 같이 놀고 싶게 만드는 매력이 있는 착한 미소천사 수연이, 장난스러운 아이 같은 모습으로 동생들을 즐겁게 해주기도 하고, 반면 연구할 때는 진중하고 무게감 있는 모습으로 무섭게 성장 중인 언젠가 꼭 성공할 것 같은 창일이, 언니, 오빠들에게 항상 예의 바르고, 늘 예쁘게 얘기해서 같이 대화를 하다 보면 좋은 말만 잔뜩 해주고 싶게 만드는, 차분함과 밝음이 공존하는 소희, 인턴 때부터 활발하게 다양한 연구주제에 관심을 가져 좋은 인상으로 남았었고, 지금도 열정과 긍정으로 많은 일들을 하나씩 해내어가는 누구보다도 강한 우리 꼬맹이 해연이, 애기 같은 얼굴로 나타난 게 엊그제 같은데 언제 이렇게 믿음직하게 성장했나 싶고, 주변 사람들에게 충고도 잘 하고 세심하게 챙겨주면서도 여전히 한번씩 귀여움도 잃지 않는 내 소중한 부사수 윤주, 항상 미소를 잃지 않아 무슨 말을 해도 다 웃으면서 받아줄 것 같은 너그러운 품성을 가진, 선글라스가 정말 잘 어울리는 echem 대표

미남이자 미래의 팹 마스터 상현이, 다른 분야 공부를 새로 도전하는게 쉽지 않았을 텐데 단단한 정신력으로 어려운 상황 속에서도 힘든 티를 잘 안 내어 멋있었고, 풍부한 경험을 바탕으로 해주는 언니의 조언과 응원이 더욱 힘이 되었던 슬 언니, 특유의 친화력과 공감능력으로 먼저 따뜻하게 다가와주어서 동생이지만 친구처럼 편하게 속 얘기를 털어놓을 수 있게 해주었고, 항상 주위 사람들을 즐겁게 해주는 분위기 메이커이자 언젠가 우리나라의 큰 손이 될 상욱이, 인턴 때부터 늦은 시간까지 남아서 공부하고 스터디도 만들어서 진행하는 모습이 참 열정적이라고 생각했고, 이번 엠티 레크레이션도 혼자 준비하느라 힘들었을텐데 너무 잘해줘서 감동을 주었던, 성실함이 빛나는 우열이, 다양한 주제에 관심을 가지고 그룹세미나에서 열심히 질문하는 모습이 인상적이었고, 조만간 연구실의 최고 인싸가 될 것 같은 예쁜 인기쟁이 민지, 모두의 귀여움을 차지하고 있지만, 똑부러진다는 이야기도 종종 들려와 반전의 다부진 매력을 가진 것 같은 민정이까지 차례로 감사의 말을 전합니다. 그리고 연구실에서 있는 동안 수많은 일들을 챙겨주신 혜정 언니 덕분에 정말 편하게 실험하고 어려움없이 생활했고, 또 많은 것들을 배웠습니다.

행복한 순간도, 힘든 순간도 많았던 지난 6년, 이렇게 소중한 분들 덕분에 많이 웃었고, 어려운 일이 닥쳤을 때도 단단하게 이겨낼 수 있었습니다. 제가 받은 고마운 마음들을 돌려드릴 수 있게 연구실을 떠난 이후에도 좋은 선배이자 후배가 되어드리고 싶습니다. 글솜씨가 부족하여 제 감사한 마음을 다 표현하지 못한 것 같아 아쉬울 따름입니다. 직접 얼굴을 마주할 기회가 앞으로 많이 남아있다고 믿고, 길었던 감사의 글을 마칩니다.